# FAKULTI : FAKULTI KEJURUTERAAN KIMIA DAN KEJURUTERAAN TENAGA TAJUK : PERBINCANGAN KEPUTUSAN PEMERIKSAAN SEMULA TESIS PELAJAR

BUTIRAN PELAJAR	KETERANGAN PELAJAR			ULASAN DAN TINDAKAN FAKULTI		KELULUSAN	
NAMA : SAEED DELAVARI  NO K/P @ ISID : 201001M10035  NO MATRIK : PK093053	<b>Bil.</b> 1. 2.	Tarikh 13/8/2014 16/11/2014	Catatan Pelajar Hantar Tesis untuk Peperiksaan Viva Keputusan C tempoh 12 bulan	1.	SPS menerima maklum balas fakulti pada 15 Ogos 2016 melalui surat rasmi bertarikh 8 Ogos 2016. Mesyuarat telah diadakan pada 2 Cgos bagi meneliti dan semakan	Setuju / Tidak Setuju Ulasan :	
PROGRAM : DOKTOR FALSAFAH (KEJURUTERAAN KIMIA) JENIS PENGAJIAN : PENYELIDIKAN	4.	8/7/2015	Terima Tesis untuk pemeriksaan semula Tesis dihantar ke Pemeriksa Dalam dan Pemeriksa Luar	3.	pelaporan data dalam tesis pelajar yang dipengerusikan oleh <b>Dekan</b> , FKT dan <b>2 orang Panel Pakar dilantik</b> <b>daripada FS dan FKT.</b> Hasil Mesyuarat semua panel		
BENTUK PENDAFTARAN : SEPENUH MASA	5.	30/11/2015	Pemeriksa Luar memberi Keputusan B1 – Semakan Penyelia		memutuskan supaya pelajar menyediakan data asal untuk semua gambarajah XRD (tesis muka surat 91),		
PENYELIA : PROF. DR. AISHAH SAIDINA AMIN	6.	28/12/2015	Pemeriksa Dalam memberi Keputusan B2 – Pembetulan 6 Bulan	4.	FTIR (tesis muka surat 148) dan XPS (tesis muka surat 151) dalam tesis. Mesyuarat Japsu adalah dipohon	Tandatangan Dekan Sekolah Pengajian Siswazah	
BIL SEM: 8 / 12	7.	9/6/2016	Terima Tesis untuk semakan Pembetulan Pertama	5.	untuk <b>menentukan keputusan asal</b> atau kedudukan pelajar dan tempoh	& Cop Rasmi	
STATUS : PEPERIKSAAN MUKASURAT : 1/1	8.	22/6/2016	Pemeriksa Dalam memberikan Keputusan Tidak Dianugerahkan Ijazah. SPS memohon		pembetulan tesis melalui pengesahan dari Fakulti.	Tarikh:	
		20,0,2010	pengesahan dakwaan Laporan Pemeriksa Dalam ke Fakulti.				

Fakulti Kejuruteraan Kimia dan Kejuruteraan Tenag**a** Universiti Teknologi Malaysi**a** 81310 Johor Bahr**u** Johor, Malaysia

Tel: +(6)07-5536034 Faks: +(6)07-5581463 http://fcee.utm.my Emel: fcee@utm.my

RUJUKAN KAMI: RUJUKAN TUAN: UTM.J.46/14.14/1/6/3/15(246)

8 Ogos 2016

Y. Bhg Prof. Dr. Zaidatun Tasir

Dekan Sekolah Pengajian Siswazah Universiti Teknologi Malaysia Johor Bahru, Johor

Assalamualaikum wrt wbt,

Y. Bhg Prof.

SEGERA

DENGAN TANGAN

With & bincapter den

-L88116-

SEMAKAN PELAPORAN DATA DALAM TESIS PELAJAR

Nama Pelajar: SAEED DELAVARI

Program: Doktor Falsafah (Kejuruteraan Kimia)

Dengan hormatnya saya merujuk kepada perkara di atas.

- 2. Sukacita dimaklumkan bahawa fakulti telah mengadakan mesyuarat mengenai semakan pelaporan data dalam tesis pelajar (Saeed Delavari) pada 2 Ogos 2016 yang dihadiri oleh 2 orang panel (pakar) yang dilantik dari Fakulti Sains dan seorang panel (pakar) dari FKT dipengerusikan oleh Dekan, Fakulti Kejuruteraan Kimia dan Kejuruteraan Tenaga.
- 3. Hasil daripada mesyuarat tersebut, semua panel telah memutuskan supaya pelajar hendaklah menyediakan 3 data asal untuk semua gambarajah XRD, FTIR dan XPS seperti yang dinyatakan di bawah, iaitu seperti mana diperlukan oleh Pemeriksa Dalaman bagi membuktikan bahawa tiada salah laku data pada tesis pelajar tersebut. Disertakan juga petikan komen dari Pemeriksa Dalaman.
  - i. XRD rujuk Figure 4.1 dan tesis mukasurat 91
    Komen: "..still did the same mistake by using incorrect figure.."
  - ii. FTIR rujuk Figure 5.4 dan tesis mukasurat 148

    Komen: "..the line of the FTIR spectra became smoother but still questionable.."
  - iii. XPS rujuk Figure 5.7(a), Figure 5.7(b) dan tesis mukasurat 151 Komen: "..cheating by using the figure that is not belong to his work.."

Sehubungan itu, pihak fakulti memohon pertimbangan Y. Bhg Prof bagi menentukan kedudukan pelajar untuk diberi tempoh pembetulan tesis.

Sekian, terima kasih.

'Berkhidmat Untuk Negara Kerana Allah"

1 J AUG Z016

...2/-

School of Graduate Studies Prof. Dr. Mohd Ghazali Bin Mohd Nawawi Prof. Madya Dr. Abdul Razak bin Rahmat

Fakulti Kejuruteraan Kimia dan Kejuruteraan Tenaga

Melalui Dekan

Fakulti Kejuruteraan Kimia dan Kejuruteraan Tenaga

Yg. Bhg Prof./Dr.,

NAMA PELAJAR

: Saeed Delavari

PROGRAM

: Doktor Falsafah (Kejuruteraan Kimia)

SEMAKAN PELAPORAN DATA DALAM TESIS PELAJAR

Perkara di atas dirujuk.

2. Untuk makluman kronologi Peperiksaan Lisan Pelajar adalah seperti perincian berikut;

Tarikh	Kronologi
16 November 2014	Viva Keputusan C tempoh 12 bulan
7 Julai 2015	Terima tesis untuk pemeriksaan semula
8 Julai 2015	Tesis dihantar ke Pemeriksa Luar dan Pemeriksa Dalam
30 November 2015	Pemeriksa Luar memberi Keputusan B1 Semakan Penyelia
28 Disember 2015	Pemeriksa Dalam memberi Keputusan B2 Pembetulan 6 Bulan
9 Jun 2016	Terima tesis untuk Semakan Pembetulan Pertama
22 Jun 2016	Pemeriksa Dalam memberi keputusan Tidak Dianugerahkan Ijazah

- 3. Seperti dibangkitkan dalam laporan pemeriksa, fakulti adalah dimohon membuat pengesahan dakwaan salah lapor data pada tesis pelajar. Sehubungan itu, pihak SPS memohon fakulti untuk melantik pakar bagi mengesahkan dakwaan ini.
- 4. Dilampirkan komen pemeriksa, cabutan tesis pelajar dan artikel jurnal yang dilampirkan oleh pemeriksa sebagai rujukan.

Sekian, kerjasama Yg. Bhg Prof./Dr. amat dihargai dan diucapkan terima kasih.

'Berkhidmat Untuk Negara Kerana Allah'

Yang benar

PROF\DR\ZAIDATUN TASIR

Dekan

Sekolah Pengajian Siswazah

UTM, Skudai

**2** 07-5537881

deansps@utm.my



### PENGESAHAN SEMAKAN PEMBETULAN TESIS (CERTIFICATION ON THE CORRECTION OF THESIS)

Tarikh (Date):

Dekan Sekolah Pengajian Siswazah Universiti Teknologi Malaysia 81310 UTM Skudai

OT A OTHER TROOP AT A	com	1 ) (D11 1 1 1 0000)	Displace and seedings.	- 6

Maklumat peperiksaan: (Diisi oleh SPS)

Tarikh viva (Date of viva): 16/11/2014

Johor	No. Faks: 07-5537800	Tempoh pembetulan (Duration for correction c - tanpa reviva	):
Tuan (Dear	r Sir),		
.0TA0JUK	TESIS (Title of Thesis) (Diisi oleh SPS): Phot	toreduction of Carbon Dioxide and Me	thane to
Formate	, Acetate Derivatives and Hydrogen	Over Immobolized Titania Nanoparti	cles and
	n-Doped Titania Nanotube Arrays		157884.778888.18884.198844.1111
NAMA PEI	LAJAR (Name of Student) (Diisi oleh SPS): Sae	eed Delavari	
FAKULTI (	(Faculty): Fakulti Kejuruteraan Kimia dau	Kejuruteraan Tenaga	
Semakan pe	embetulan: Pertama / <b>Kedua*</b> (Correction verifica	ntion: First/Second*)(Diisi oleh SPS)	
telah i pemeri the ned be awa sedikit dianug	iksa dan saya mengesyorkan pelajar di atas dianu ccessary corrections recommended by the Panel arded Master/Phd* degree) pembetulan yang hanya perlu disahkan oleh	and satisfied that the candidate):  thap sebagaimana yang dicadangkan oleh panel gerah Ijazah Sarjana/Doktor Falsafah (has done all of Examiners and I recommend that the candidate penyelia dan saya mengesyorkan pelajar di atas sections need to be verified by the supervisor and I	(Initial)
2. Pelajar out all i. ii.	the neccessary corrections recommended by the in membuat pembetulan semula (redo correction)	n):hari/bulan*( <i>days/months</i> *).	ed to carry
iii.	tidak dianugerah Ijazah (not be awarded)		
3. Penyata	aan Lain (Other Remarks - if any): Pembet a kali. Untik komen laujut	ulan felah dibual sebanyal Sila lihat laupiran	<u>د</u>

dua	a Kali	. UNTIL	comen	Kar ( u)	r
				7	
Pengesahan d	libuat oleh	(Certified	<i>by)</i> :	••••	
Nama (Name)	): (	Ņ		·····	
Pemeriksa Lu	ıan/Pemeri	ksa Dalam	<b>&gt;</b>		

(External Examiner/Internal Examiner)\*

PROFESSOR DR. AISHAH ABBUL JALIL Alamat (Address): Department of Chemical Engineering
Faculty of Chemical and Energy Engineering Jaivarsiti Telmologi Malaysia 81310 Utm Johor Bahru, John

#### Perhatian (Attention):

Boleh dihantar dengan faks (07-5537800) untuk kegunaan segera tetapi salinan asal MESTI dihantar ke Sekolah Pengajian Siswazah. (This certification may be faxed (07-5537800) for urgent usage but the original copy MUST be sent to the School of Graduate Studies).

<sup>\*</sup>Sila potong yang tidak berkenaan (\*Delete where not applicable)

# Conclusion from Internal Examiner for Second-Correction for PhD Thesis of Saeed Delavari

Title: Photoreduction of Carbon Dioxide and Methane to Formate, Acetate Derivatives and Hydrogen Over Immobilized Titania Nanoparticles And Nirogen-Doped Titania Nanotubes Arrays

Examiner: Prof. Dr Aishah Abdul Jalil (Internal)

The conclusion from internal examiner regarding to Saeed's response for each comments are as follows:

No.	Examiner Comment	Conclusion from Examiner	Remark (Latest thesis)
The	candidate should get the "real" figures for comments below.		
1.	Page 79: Move the Fig. 3.4 into Chapter 4 (Result and Discussion).	OK.	Page 94
2.	Page 92: The JCPDS 84-1286 shown in Fig. 4.1 is wrong.	The student still did the same mistake by using the incorrect figure. Unfortunately, the student did not understand what the meaning of the JCPDS figure. This is really a ridiculous mistake because as a PhD student who is doing this kind of main analysis (XRD) in the catalyst area, he should know the exact figure.  The reference for the answer of this question is attached, and many images could be also found from google image.	Page 91

3.	Page 149: Run and show the "real" FTIR spectra for Fig. 5.4.	In the 1 <sup>st</sup> correction, the student sketched the FTIR spectra by himself (Page 149), which is a very disgraceful mistake as a PhD student.  In this 2 <sup>nd</sup> correction, the line of the FTIR spectra became smoother but still questionable.  The reference for the nitrogen-doped TiO <sub>2</sub> is attached.	Page 148
4.	Check all the references in the thesis and make sure that they are appropriate for the related sentences.	OK.	
3	Page 152: Show the appropriate XPS figure for the interaction between the TiO <sub>2</sub> and Nitrogen.	The Figure 5.7b is not same with the Figure 5.7a. Thus, again the student also did the ridiculous cheating by using the figure that is not belong to his work.  The references for the nitrogen-doped TiO <sub>2</sub> are also attached.	Page 151
6.	Page 153: Delete the bullet in Fig 5.7.	OK.	
7.	Page 154: Combine the Fig. 4.3 and Fig. 5.8 to show the changes before and after doping with N. Make sure you get the "real" figure for all the figures.	OK.	Page 154

## Kepada yang Berkenaan,

## Komen umum dari saya:

Pada pendapat saya pelajar tidak layak dianugerahkan PhD dari UTM kerana sebab2 berikut:

- 1) Pelajar didapati menipu (plagiarism) dalam viva beliau, telah dikemukakan bukti yang sah iaitu paper yang beliau tiru dan diakui oleh panel viva semua tetapi pelajar masih tidak mengaku (sila rujuk komen pengerusi).
- 2) Viva terpaksa diberhentikan oleh pengerusi separuh jalan kerana pelajar banyak tidak dapat memberikan jawapan yang sepatutnya semasa viva.
- 3) Walupun demikian, kami para penilai dan pengerusi viva masih setuju untuk memberi peluang kedua kepada pelajar dengan memberi keputusan C kepada pelajar untuk membuat pembetulan. Akan tetapi, dalam 2<sup>nd</sup> correction ini, saya mendapati ada lagi data yang tidak jelas (tipu lagi). Saya sertakan beberapa bahan rujukan untuk pihak SPS rujuk kepada mereka yang lebih pakar dalam bidang pencirian bahan contohnya para pensyarah dari Fakulti Sains.

Oleh itu kesimpulan dari saya, pelajar telah banyak kali menipu data walaupun telah diberi peluang untuk membetulkannya, maka bagi saya beliau tidak layak dianugerahkan PhD demi menjaga kualiti penganugerahan PhD di UTM.

Sekian terima kasih.

PROFESSOR OR. AISHAH ABDUL JALIL Department of Chemical Engineering Faculty of Chemical and Energy Engineering Universiti Teknologi Malaysis. #1310 Utm Joher Bahru. Johor.

22/6/2016

# Phase Characterization of TiO<sub>2</sub> Powder by XRD and TEM

Kheamrutai Thamaphati\*, Pichet Limsuwani and Boonlaer Ngotawornchai2

#### **ABSTRACT**

In this study, the commercial  $TiO_2$  nanopowder and micropowder of anatase phase and rutile phase have been characterized by x-ray diffraction (XRD) and transmission electron microscopy (TEM). XRD patterns of nano- $TiO_2$  in rutile and anatase phases exhibit broad peaks whereas both phases of micro- $TiO_2$  demonstrate very sharp peaks. TEM images show that the grain size of  $TiO_2$  micropowders and  $TiO_2$  nanopowders are 0.3-0.7  $\mu m$  and 10 nm, respectively. The selected-area electron diffraction patterns of  $TiO_2$  nanopowders in rutile and anatase phases are consistent with XRD results.

Key words: TiO2, anatase, rutile, micro and nanopowders, TEM, XRD

#### INTRODUCTION

Titanium dioxide or titania (TiO<sub>2</sub>) was first produced commercially in 1923. It is obtained from a variety of ores. The bulk material of TiO<sub>2</sub> is widely nominated for three main phases of rutile, anatase and brookite (Kim *et al.*, 2005). Among them, the TiO<sub>2</sub> exists mostly as rutile and anatase phases which both of them have the tetragonal structures. However, rutile is a high-temperature stable phase and has an optical energy band gap of 3.0 eV (415 nm), anatase is formed at a lower temperature with an optical energy band gap of 3.2 eV (380 nm) and refractive index of 2.3 (Brady, 1971).

TiO<sub>2</sub> is mainly applied as pigments, adsorbents, catalyst supports, filters, coatings, photoconductors, and dielectric materials. In recent years, TiO<sub>2</sub> has been well known as a semiconductor with photocatalytic activities and has a great potential for applications such as environmental purification, decomposition of

carbonic acid gas, and generation of hydrogen gas (Zhang et al., 2000). In most of these cases, the size of the TiO<sub>2</sub> particles is an important factor affecting the performance of the materials. It is not surprising; therefore, that much research has been focused upon the reduction of the particle size. Much effort has been devoted to the preparation of TiO<sub>2</sub> nanopowders, including solgel route, homogeneous precipitation, hydrothermal methods, flame synthesis and relatively new molten salts method (Bilik and Plesch, 2007). They were usually found that different routes often produced different results. Even for the same route, using different amount of the starting materials, the obtained powder size is different (Li et al., 2002).

Consequently, phase and particle size are the important parameters that influence physical properties of material. Several techniques could be used for the investigation of them. However, the particle size determination can be based on direct observation of particles by transmission

Department of Physics, Faculty of Science, King Mongkut's University of Technology Thonburi, Bangkok 10140, Thailand.

Scientific and Technological Research Equipment Centre, Chulalongkorn University, Bangkok 10330, Thailand.

Corresponding author, e-mail: opticslaser@yahoo.com

electron microscopy (TEM) or scanning electron microscope techniques, in this case, we can also receive the important information on the shape of particles. Data on particle size can be obtained by X-ray diffraction (XRD) technique as the particle size is related to the diffraction peak broadening. It is important to note that TEM and XRD methods allow not only to measure the particle size, but also to identify crystalline phases.

### MATERIALS AND METHODS

Four commercial TiO<sub>2</sub> samples used in this experiment were provided by Aldrich: (i) 99.7 % anatase, nanopowder; (ii) 99.8 % anatase, micropowder; (iii) 99.5 % rutile, nanopowder; (iv) 99.9 % rutile, micropowder.

XRD measurements were performed on the Bruker D8 Advance diffractometer operating in the reflection mode with Cu-K $\alpha$  radiation (35 kV, 30 mA) and diffracted beam monochromator, using a step scan mode with the step of 0.075° (2 $\theta$ ) and 4 s per step. Diffraction patterns of both anatase and rutile TiO<sub>2</sub> powders were compared with reference to JCPDS database. Additionally, the morphology of the powder was observed by

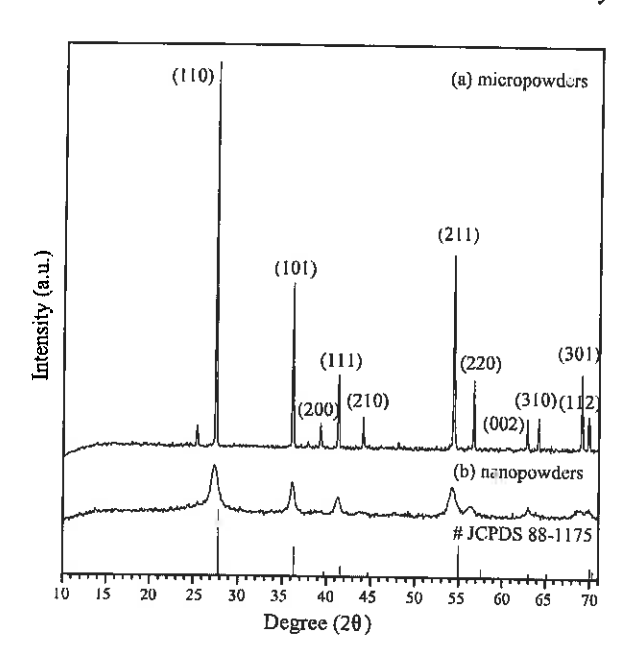


Figure 1 X-ray diffraction of rutile TiO<sub>2</sub> (a) micropowders and (b) nanopowders.

TEM with a JEOL JEM-2100 ultra high resolution TEM operating at 160 kV.

#### RESULTS AND DISCUSSION

#### **XRD**

XRD patterns of nano-TiO2 and micro-TiO<sub>2</sub> in rutile and anatase phases are shown in Figure 1 and Figure 2, respectively. In Figure 1, XRD patterns exhibited strong diffraction peaks at 27°, 36° and 55° indicating TiO2 in the rutile phase. On the other hand, in Figure 2, XRD patterns exhibited strong diffraction peaks at 25° and  $48^{\circ}$  indicating  $TiO_2$  in the anatase phase. All peaks are in good agreement with the standard spectrum (JCPDS no.: 88-1175 and 84-1286). From Figure 1 and Figure 2, they were shown that the diffraction pattern peak intensity of the TiO2 increases with increasing particles size. These results suggested that the nano-TiO2 powder is composed of irregular polycrystalline. Amorphous revealed a broad pattern with low intensity; however, the effect of the amorphous materials on the broadening of the XRD patterns of nanosized TiO<sub>2</sub> is negligible.

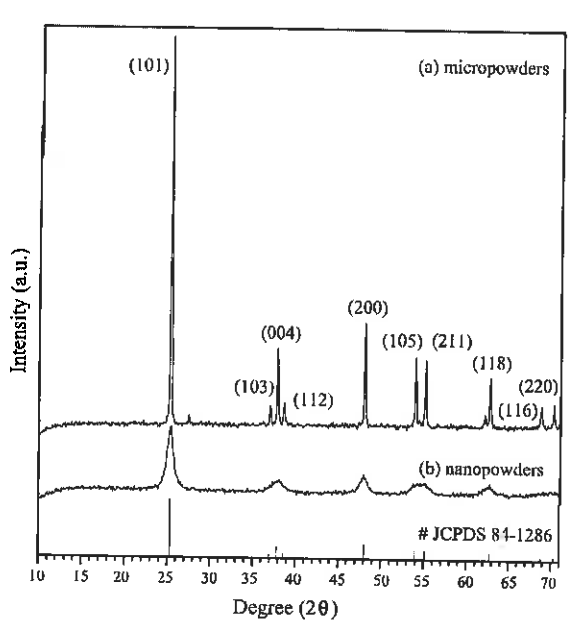


**Figure 2** X-ray diffraction of anatase TiO<sub>2</sub> (a) micropowders and (b) nanopowders.



#### **TEM**

TEM was used to further examine the particle size, crystallinity and morphology of samples. TEM bright field images of TiO<sub>2</sub> micropowders in rutile and anatase phases are shown in Figure (3a) and (4a), respectively. It is clearly seen that the TiO<sub>2</sub> powders in rutile phase consist of both spherical and rod shapes but the particle of TiO<sub>2</sub> powders in anatase phase are mostly spherical morphology. Furthermore, it can be estimated that the particle size of samples in Figure (3a) and (4a) are microscale with the grain size about 0.3-0.7 μm.

nanopowders in rutile and anatase phases are shown in Figure (3b) and (4b), respectively. It can be estimated that the particle size of powders in Figure (3b) and (4b) are nanoscale with the grain size lese than 10 nm. The corresponding selectedarea electron diffraction (SAED) patterns of nano-TiO<sub>2</sub> powders in rutile and anatase phases are shown in Figure (3c) and (4c), respectively. These are in agreement with XRD results in Figure (1b) and (2b), respectively. In Figure (3c), the SAED patterns of nano-TiO<sub>2</sub> powders in rutile phase shows spotty ring patterns without any additional

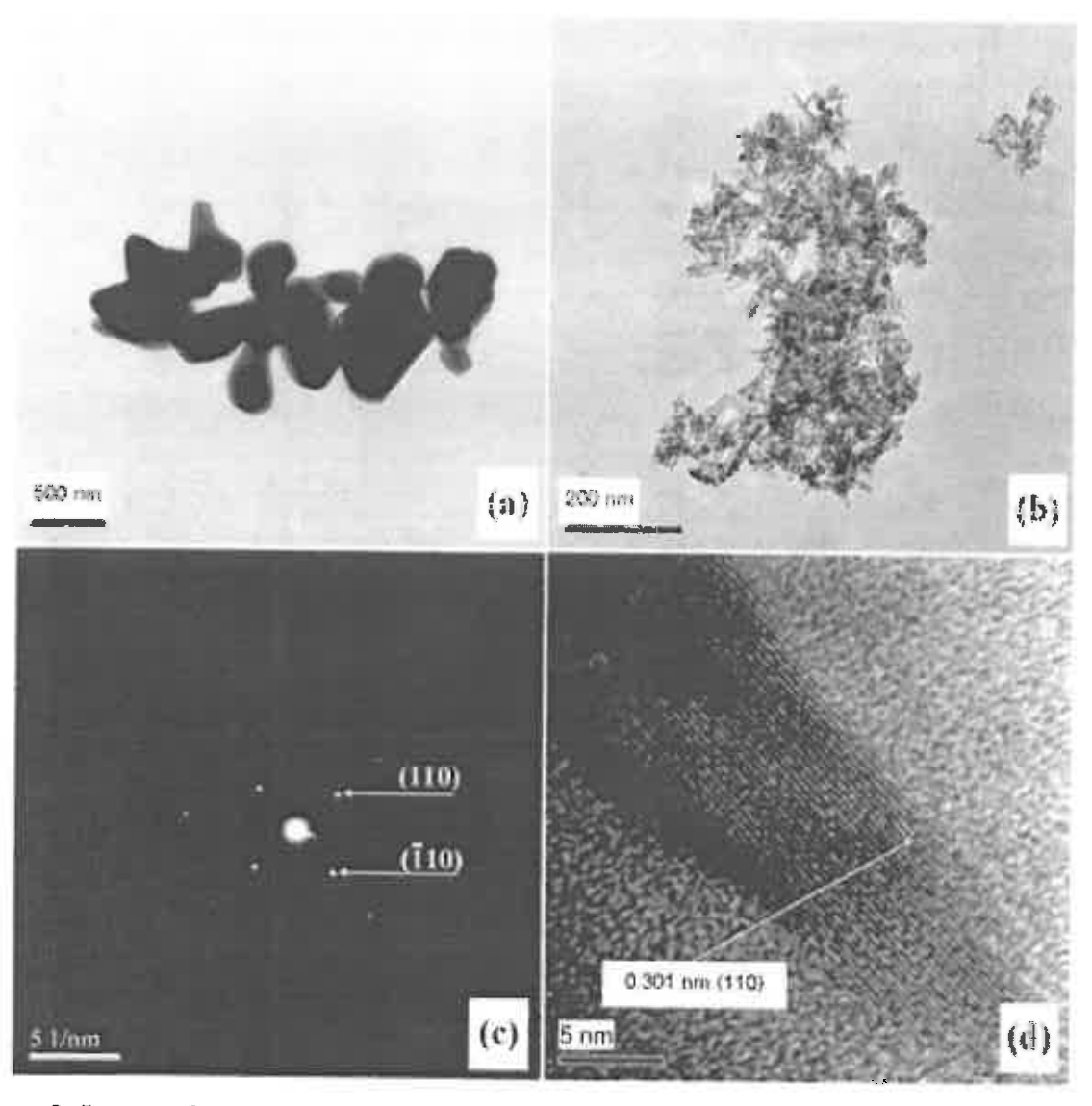


Figure 3 Images of rutile phase. (a) TEM image of micro-TiO<sub>2</sub> powder; (b) TEM image of nano-TiO<sub>2</sub> powder; (c) SAED pattern of nano-TiO<sub>2</sub> powder and (d) HRTEM image of nano-TiO<sub>2</sub> powder.

diffraction spots and rings of second phases, revealing their well crystalline. On the other hand, the SAED patterns of nano-TiO<sub>2</sub> powders in anatase phase (Figure (4c) shows that the brightness and intensity of polymorphic ring is weak, so they are poorly crystallized and partly amorphous.

The crystallinity of nano-TiO<sub>2</sub> powders can also be observed by phase-contrast images or Moire patterns. Figure (3d) and (4d) show crystal lattice planes of nano-TiO<sub>2</sub> in rutile and anatase phases, respectively. It is seen that, for rutile phase,

only one crystal lattice plane(110) with d-spacing of 0.301 nm is obtained, whereas those of anatase give many crystal lattice planes with d-spacing of 0.313 nm for the plane (101).

#### CONCLUSION

In this work, a study has been carried out on the identification of phase and particle size of TiO<sub>2</sub> powders using XRD and TEM techniques. All high purities samples were commercial TiO<sub>2</sub>. From the results, X-ray diffraction patterns can

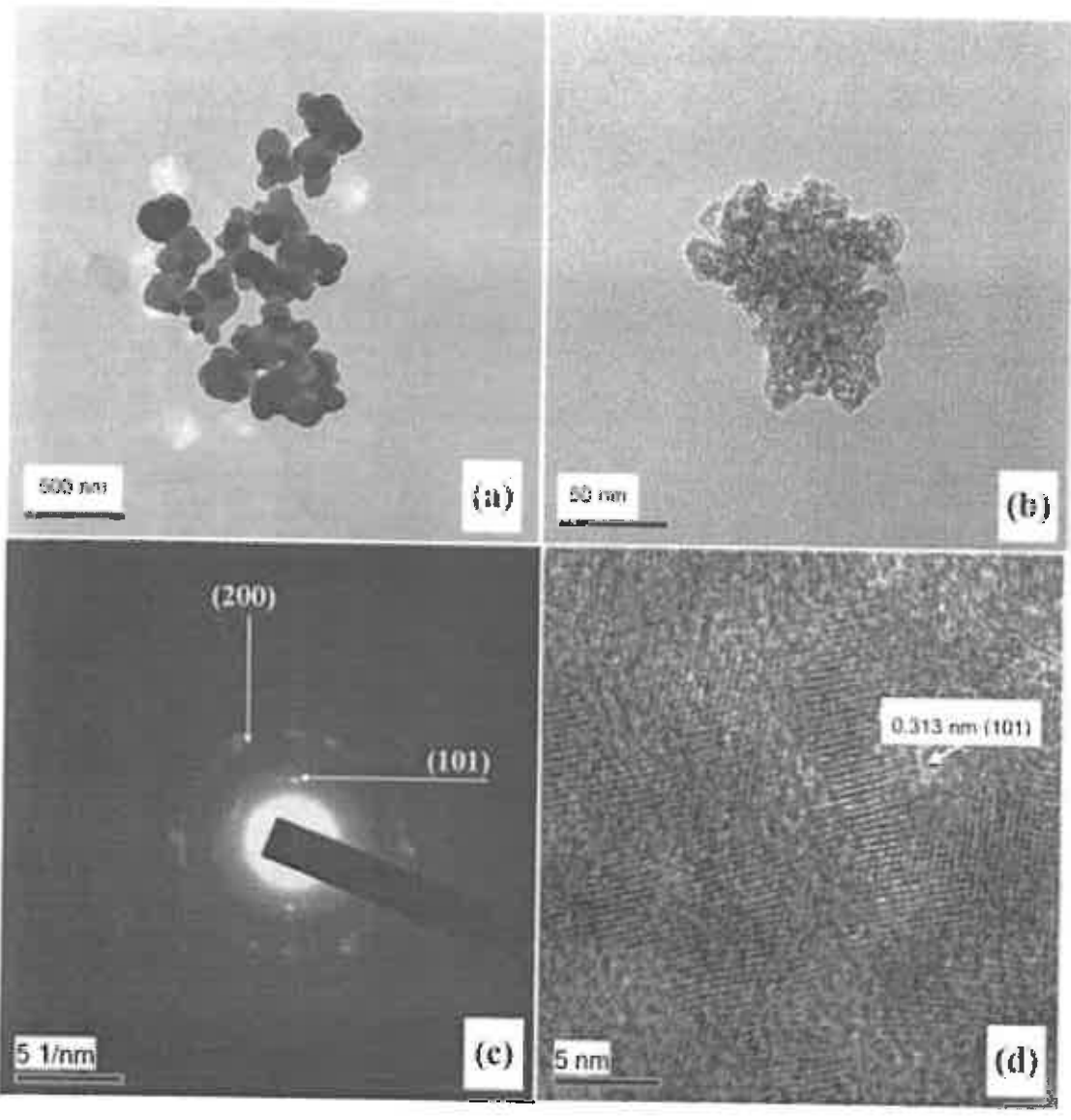


**Figure 4** Images of anatase phase. (a) TEM image of micro-TiO<sub>2</sub> powder; (b) TEM image of nano-TiO<sub>2</sub> powder; (c) SAED pattern of nano-TiO<sub>2</sub> powder and (d) HRTEM image of nano-TiO<sub>2</sub> powder.

confirm the TiO<sub>2</sub> phases. Furthermore, the particle size can be clearly indicated by characteristic of XRD pattern; the diffraction pattern peak intensity of the TiO<sub>2</sub> increases with increasing particles size. Additionally, TEM was used to further examine the crystallite/particle size, the crystallinity and morphology of samples. TiO<sub>2</sub> powders in rutile phase consist of both spherical and rod shape; on the contrary, the particle of TiO<sub>2</sub> in anatase phase has mostly spherical morphology.

#### **ACKNOWLEDGEMENTS**

This work is financially supported by the Department of Physics, the Faculty of Science, King Mongkut's University of Technology Thonburi and the Nano Technology Center (NANOTEC).

#### LITERATURE CITED

- Bilik, P. and G. Plesch. 2007. Mechanochemical synthesis of anatase and rutile nanopowders from TiOSO<sub>4</sub>. Mater. Lett. 61: 1183-1186.
- Brady, G.S. 1971. **Materials Handbook**. New York: McGraw-Hill.
- Kim, T.K., M.N. Lee, S.H. Lee, Y.C. Park, C.K. Jung and J.H. Boo. 2005. Development of surface coating technology of TiO<sub>2</sub> powder and improvement of photocatalytic activity by surface modification. Thin Solid Films 475: 71-177.
- Li, B., X. Wang, M. Yan and L. Li. 2002. Preparation and characterization of nano-TiO<sub>2</sub>Powder, Mater. Chem. Phys. 78: 184-188.
- Zhang, Q., L. Gao and J. Guo. 2000. Effect of hydrolysis conditions on morphology and crystallization of nanosized TiO<sub>2</sub> powder. J. Eur. Ceram. Soc. 20: 2153-2158.





Contents lists available at ScienceDirect

# Applied Surface Science

journal homepage www elsovier com/locate apsoso



# Dynamic photocatalytic reduction of CO<sub>2</sub> to CO in a honeycomb monolith reactor loaded with Cu and N doped TiO<sub>2</sub> nanocatalysts



Muhammad Tahir , Beenish Tahir

Chemical Reaction Engineering Group (CREG), Department of Chemical Engineering, Faculty of Chemical and Energy Engineering, Universiti Teknologi Malaysia, 81310 UTM, Skudai, Johor Baharu, Johor, Malaysia

#### ARTICLE INFO

Article history:
Received 3 January 2016
Received in revised form 16 March 2016
Accepted 17 March 2016
Available online 19 March 2016

Keywords:
Dynamic CO<sub>2</sub> reduction
H<sub>2</sub> reductant
Cu-N doping
Cordierite honeycomb monolith
Continuous operation

#### ABSTRACT

Cordierite honeycomb monoliths loaded with N/TiO<sub>2</sub> and Cu/TiO<sub>2</sub> nanocatalysts for dynamic photocatalytic CO<sub>2</sub> reduction with H<sub>2</sub> to CO in a continuous photoreactor illuminated with UV-light irradiations have been investigated. The nanocatalysts, loaded over the monoliths channels using sol-gel dip-coating method, were characterized by X-ray diffraction (XRD), field emission scanning electron microscopy (FESEM), N<sub>2</sub> adsorption-desorption, X-ray photoelectron spectroscopy (XPS), UV-vis diffuse reflectance and photoluminescence (PL) analysis. Crystalline and anatase TiO<sub>2</sub> structure with nanoparticles evenly supported over the cordierite monolith channels were observed. Cu and N presented over TiO<sub>2</sub>, shifted band gap energy towards visible region and hindered charges recombination rate. Loading Cu and N greatly improved TiO<sub>2</sub> photoactivity for dynamic CO<sub>2</sub> reduction to CO. Due to high photoactivity and selectivity, Cu/TiO<sub>2</sub> assisted system yielded 14 times higher CO than the N/TiO<sub>2</sub> and 64 times the amount of copper observed over pure TiO<sub>2</sub> in a continuous operation of photoreactor. This significant improvement in Cu/TiO<sub>2</sub> activity was noticeable due to efficient trapping and transport of electrons by Cu-metal. With unique properties, N/TiO<sub>2</sub> showed good activity for continuous CO<sub>2</sub> reduction to CH<sub>4</sub>. In addition, a photocatalytic reaction mechanism is proposed to understand the experimental results over Cu and N modified TiO<sub>2</sub> catalysts in a continuous operation of photoreactor.

© 2016 Elsevier B.V. All rights reserved.

#### 1. Introduction

The rise in atmospheric  $CO_2$  concentration due to fossil fuel combustion is causing major concerns of energy sustainability and environmental protection [1]. Numerous efforts are devoted to  $CO_2$  capture, storage and utilization; yet photocatalytic  $CO_2$  transformation to fuels provides one prospective path for the storage of solar energy to chemical energy [2.3]. During the recent decades, photocatalytic  $CO_2$  reduction to carbon monoxide [4], methane [2], methanol [5] and hydrocarbons [ $\overline{v}$ ] over different types of semiconductor materials has been consistently drawing increasing attention. The state-of-the-art photocatalytic  $CO_2$  reduction, however, requires photocatalysts that meet certain stringent criteria [7–9].

Most of the research on CO<sub>2</sub> photoreduction has been related to TiO<sub>2</sub> due to its numerous advantages which include low cost, avail-

Non-metallic elements such as C, S, F and N are considering as economical dopants to improve TiO<sub>2</sub> photoactivity. However, special considerations were paid for N since it has particular doping property and visible light sensitivity. In different studies, it has been reported that N shifted TiO<sub>2</sub> band gap energy for efficient CO<sub>2</sub> reduction to fuels under visible light irradiations [22,23]. However, there is a lack of systematic study about the function of N/TiO<sub>2</sub>

able in excess, nontoxic, chemically/thermally stable and strong oxidative potential [10,17]. However, TiO<sub>2</sub> is active only under UV-light due to its wide band gap energy (~3.2 eV for anatase). The shorter lifetime of photo-generated electron-hole pairs in TiO<sub>2</sub> is another challenge, resulting in lower photoactivity. Different noble metals such as Au, Ag, Cu, Ni, and Pt are considered efficient to improve TiO<sub>2</sub> photoactivity and selectivity [12–15]. The noble metals serve as electron traps to suppress the recombination rate of the photo-generated charges. Among all, copper has been reported as an efficient dopant to enhance TiO<sub>2</sub> photoactivity for selective CO<sub>2</sub> reduction [16–19]. Incorporating Cu-metal ions (Cu°, Cu<sup>+</sup>, Cu<sup>2+</sup>) into TiO<sub>2</sub> could lead to stimulate electron transfer between metal/semiconductor junction to improve photoactivity [20]. In addition, copper has low price, non-toxicity, environmental acceptability and good photoactivity [21].

<sup>\*</sup> Corresponding author. Permament address: Department of Chemical Engineering, COMSATS Institute of Information Technology Lahore, Defence Road, Off Raiwind Road Lahore, Pakistan.

E-mail addresses: mitable rch me, win, my, bit thirs yahoo, core (M. Tahir).

 Table 1

 Summary of physicochemical characteristics and products analysis over various catalysts.

Sample	BET Pore volume Crystal size $E_{bg}$ Yield rate- ( $\mu$ mole g-catal. $^{-1}$ h $^{-1}$ )					Quantum yield <sup>e</sup> (%)			
	$(m^2/g)$	(cm <sup>3</sup> /g)	(nm)	(eV)	CO	CH <sub>4</sub>	со	CH₄	со
TiO <sub>2</sub>	42	0.13	19	3.12	12	0.46	96.31	3.69	0.0013
3% N/TiO <sub>2</sub>	47	0.15	14	3.06	56	2.15	96.30	3.70	0.0061
3% Cu/TiO <sub>2</sub>	50	0.18	13	3.02	763	4.20	99.45	0.55	0.0826

<sup>a</sup> Crystal size calculated using Scherrer equation based on 101 peak of TiO<sub>2</sub>.

b Band gap energy calculated using Tauc equation, from a plot of  $(\alpha h v)^2$  versus photon energy (hv).

Yield rate of  $C_i(\frac{\mu mole}{g-catalyst,h}) = \frac{\mu mole of C_i produced}{(wt. of catalyst, time)}$ .

d Selectivity of product  $C_i(\%) = \frac{\text{moles of } C_i \text{ inproduct}}{\text{Total moles of C produced}} \times 100.$ 

<sup>e</sup> Quantum yield of CO(%) =  $\frac{2 \times \text{moleofCOproductionrate(mole/s)}}{\text{moleoglypotonsintensity(mol/s)}} \times 100$ .

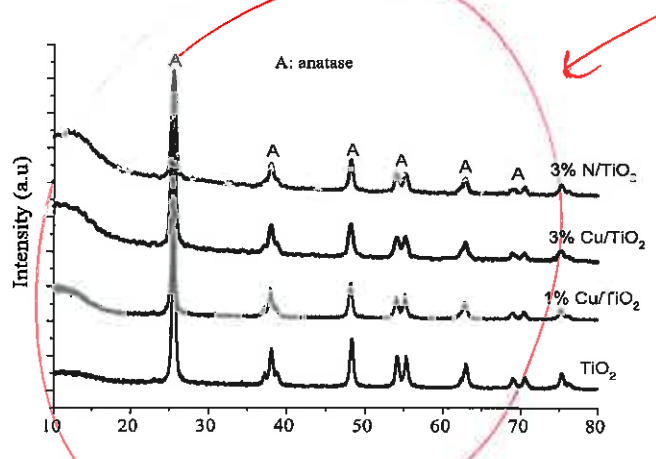


Fig. 1. XRD patterns of pure  $TiO_2$ ,  $Cu/TiO_2$  and  $N/TiO_2$  samples.

under UV-light irradiations. It is important to make clear the role of N in  $TiO_2$  for  $CO_2$  photoreduction under UV and visible light irradiations. Besides, there are limited reports up to date on dynamic and selective  $CO_2$  photoreduction with  $H_2$  to CO; therefore, it is noteworthy to explore  $CO_3$  and  $CO_4$  doped  $CO_5$  catalysts.

On the other hand, if the exposed surface area of catalyst is lower and if the photons are not effectively distributed over the photocatalyst than the system efficiency will be lowered [24.25]. During the past years, slurry photoreactors in liquid phase are the most used in CO<sub>2</sub> reduction, but they have poor light penetration in the suspension [26]. In addition, it is very difficult to achieve uniform light distribution over the entire catalyst surface in slurry systems, which is critical to activate photocatalyst [27]. Due to the complex nature of photocatalytic reactions, the efficient interaction between light irradiation, reactants and catalyst is one of the major challenges in the design of photoreactors. The catalyst support is efficient only if it has a high ratio of active surface area to reactor volume, efficient light distribution and greater photonic efficiency [28].

Presently, gas phase and in particular structured photocatalytic systems has been suggested for many photocatalytic processes [29]. Among the structured supports, monolithic substrates are exploited for many industrial processes due to unique structure with high surface area to volume ratio, thus could increase interaction between light irradiation and catalyst. We have recently reported gas phase photocatalytic CO<sub>2</sub> reduction in a batch mode monolith photoreactor, where Au-In/TiO<sub>2</sub> [30] and Ni-In/TiO<sub>2</sub> [31] photocatalysts were immobilized on the monolith channels. With this new configuration, enhanced yield rate, improved selectivity and high photonic efficiency were attained.

In this study, dynamic photocatalytic  $CO_2$  reduction with  $H_2$  to CO over  $Cu/TiO_2$  and  $N/TiO_2$  nanocatalysts loaded on cordierite honeycomb monoliths in a continuous photoreactor operation has been investigated. The effects of Cu and Cu on the photocatalytic

different with Socied XXIII all Some lab )

properties of  $TiO_2$  based structured systems for selective  $CO_2$  reduction via reverse water gas shift (RWGS) reaction under UV light irradiation are discussed in detail. The quantum yield and reaction pathways were analyzed to elucidate the role of each metal in the  $CO_2$  reduction process.

#### 2. Experimental

#### 2.1. Photocatalyst preparation

Cordierite honeycomb monoliths (100 cells per square inch, cylindrical in shape) measuring 20 mm in length and 60 mm diameter purchased from China were used. The nanocatalysts were prepared and supported over the monolith channels using modified sol-gel method as reported previously [3]. In a typical procedure, 15 mL acetic acid (1 M) was added dropwise to an aqueous solution of 20 mL titanium tetra isopropoxide ( $\text{Ti}(C_3H_7O)_4$ ) in 60 mL isopropanol ( $C_3H_7O$ ). The obtained mixture was stirred at ambient temperature for 12 h to get titanium sol. Next, an adequate amount of copper nitrate or urea dissolved in deionized water was added to titanium sol and then aged for another 6 h to get clear sol. The sol obtained was poured into a glass container for coating over the monolith channels.

Before catalyst loading, monoliths were washed with acetone and isopropanol to remove any organic material, dried at 80°C for 12 h and then cooled to room temperature. The initial weight of the dried monolith was noted and then dipped into the titanium sol to a specific time for the catalyst coating. The excess sol was blown off using hot compressed air. The coating procedure was repeated to reach an expected catalyst loading. The honeycomb monoliths were finally calcined at 500°C for 5 h (5°C min<sup>-1</sup>). The amount of catalyst loaded was calculated by subtracting the final weight of catalyst coated monolith from the initial weight of bare monolith. For every coating, three readings were noted and their average values are reported.

#### 2.2. Catalyst characterization

The crystalline phase was investigated using powder x-ray diffraction (XRD). The XRD patterns were collected between 10–80° of 20 with a step size 0.05° and a step time of 1 s using a Bruker D8 advance diffractometer equipped with Cu-  $K\alpha$  incident radiation ( $\lambda$ = 1.54 A°, 40 kV and 40 mA). The morphology of the samples was examined by field emission scanning electron microscopy (FESEM, Hitachi SU8020). The elemental states were analyzed using X-ray photoelectron spectroscopy (XPS, Axis Ultra DLD Shimadzu). The XPS spectrum was calibrated with respect to the binding energy of the C1s signal at 284.60 eV as the internal standard. The surface area measurements (BET) of the photocatalyst powders were carried out using  $N_2$  adsorption-desorption isotherms with Surfer-

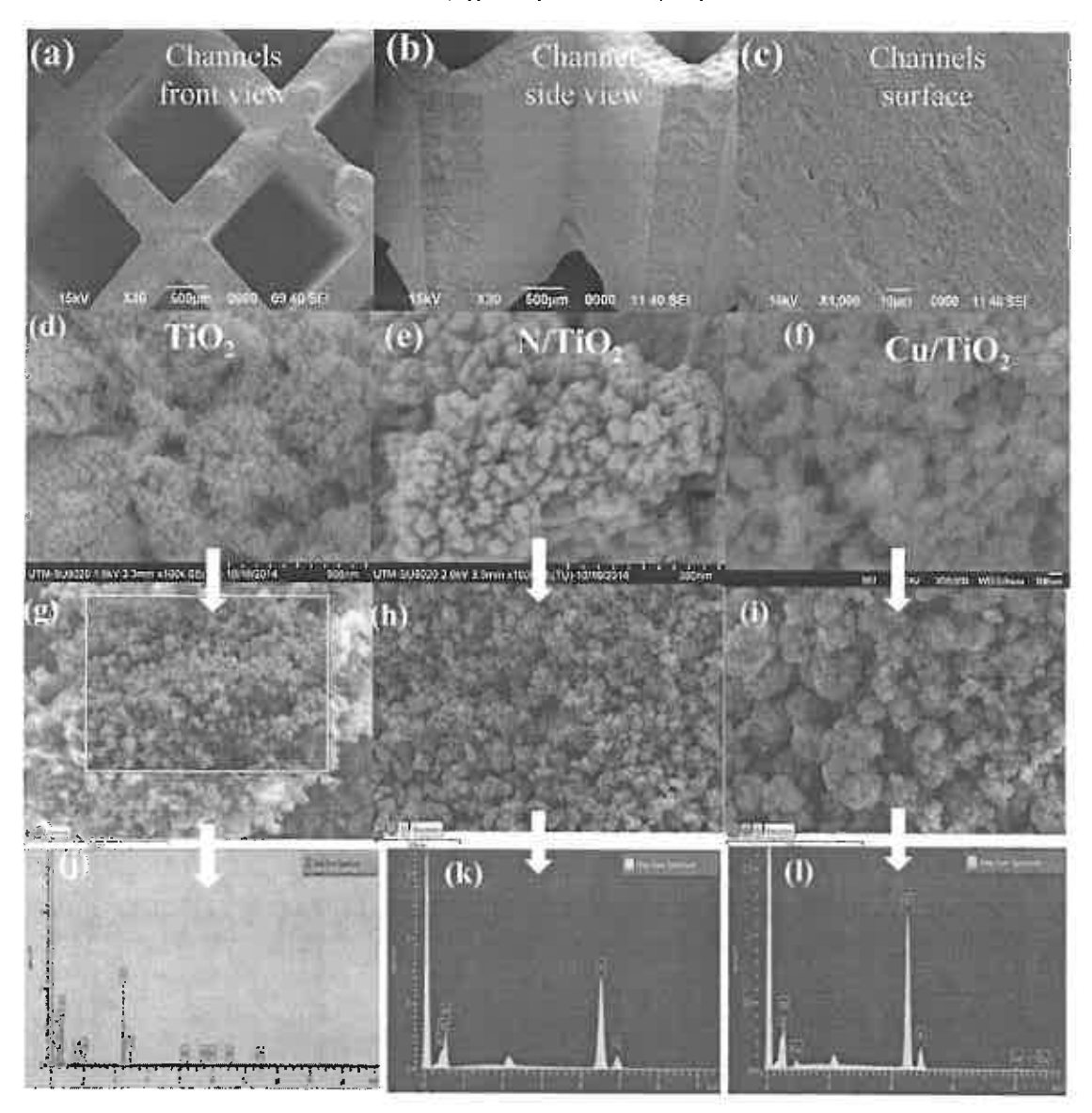


Fig. 2. SEM and FESEM images of cordierite honeycomb substrate loaded with catalysts nanoparticles; (a–c) SEM images of top and side view of catalyst loaded cordierite honeycomb channels, (d–f) FESEM images of TiO<sub>2</sub>, N/TiO<sub>2</sub> and Cu/TiO<sub>2</sub> nanoparticles, (g–i) elemental mapping of TiO<sub>2</sub>, N/TiO<sub>2</sub> and Cu/TiO<sub>2</sub> samples, (j–l) EDX plots of TiO<sub>2</sub>, N/TiO<sub>2</sub> and Cu/TiO<sub>2</sub> nanoparticles.

Thermo-Scientific after degassing at 250 °C for 4 h. UV-vis diffuse reflectance absorbance spectra were determined in the wavelength range of 200–800 nm using UV-vis spectrophotometer (Agilent, Cary 100) equipped with an integrated sphere. The charges recombination rate was analyzed using PerkinElmer LS 55 Luminescence Spectrometer.

#### 2.3. Photocatalytic activity testing

The design of continuous monolith photoreactor used in this work was described in detail in our previous work [29]. The reactor was consisted of a stainless steel cylindrical vessel with a total volume  $150\,\mathrm{cm}^3$ , equipped with a quartz window and a reflector lamp located above the reactor. The catalyst coated cordierite honeycomb monoliths (100CPSI, L=20 mm, d=60 mm) were inserted inside the reactor chamber. 200 W Hg reflector lamp was used as a source of light with a maximum light intensity of  $150\,\mathrm{mW\,cm}^{-2}$  and wavelength  $254\,\mathrm{nm}$ . An optical process monitor ILT OPM-1D

and a SED008/W sensor was used to measure the light intensity. The reactor was purged using helium (He) flow before gas mixtures ( $CO_2$  and  $H_2$ , purity = 99.99%) was continuously passed through the reactor at a flow rate of 20 mL/min. The operating conditions used were  $CO_2/H_2$  feed ratio 1.0, temperature 100 °C and pressure 1 atm. All the experiments were carried out in a continuous mode of operation and products were analyzed after regular intervals.

The CO $_2$  reduction products were analyzed using an on-line gas chromatograph (GC-Agilent Technologies 6890 N, USA) equipped with TCD and FID detectors. FID detector was connected with a HP-PLOT Q capillary column (Agilent, length 30 m. ID 0.53 mm, film 40  $\mu$ m) for separation of C $_1$ –C $_6$  paraffin and olefins hydrocarbons, alcohols and oxygenated compounds. The TCD detector was connected to UCW982, DC-200, Porapak Q and Mol Sieve 13X columns. Porapak Q and DC-200 columns were used for separation of C $_1$ –C $_5$  compounds and light gasses (H $_2$ , O $_2$ , N $_2$ , CO) were separated using MS-13X columns.

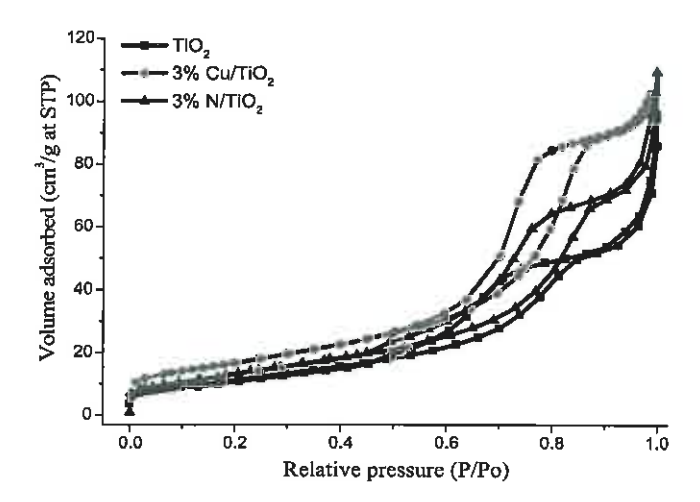


Fig. 3. N<sub>2</sub> adsorption-desorption isotherms of TiO<sub>2</sub>, N/TiO<sub>2</sub> and Cu/TiO<sub>2</sub> samples.

#### 3. Results and discussion

#### 3.1. Nanocatalysts characterization

XRD patterns of TiO<sub>2</sub>,  $Cu/TiO_2$  and  $N/TiO_2$  samples are presented in Fig. 1. Pure crystalline and anatase phase  $TiO_2$  could be seen in all

the TiO<sub>2</sub> samples. All the peaks of TiO<sub>2</sub> and Cu/N loaded TiO<sub>2</sub> samples were identical, thus shift in peaks were not observed. The peaks attributable to Cu or N in metal or oxide states were not detected, possibly due to the low amount, or they were uniformly distributed inside the TiO<sub>2</sub> structure [32,33]. The crystallite sizes were estimated from the XRD patterns using Scherer equation and the data is presented in Table 1. The TiO<sub>2</sub> crystallite size was gradually reduced with Cu and N loading. This was probably Cu and N presented over the TiO<sub>2</sub> structure prohibited crystal growth, resulting in reduced crystallite sizes [4,32].

The morphology of cordierite support, catalyst particles, and metals distribution is presented in Fig. 2. SEM micrographs in Fig. 2(a-c) depict catalyst deposited evenly over the cordierite surface with no broken layer. The sol-gel dip-coating method used to support catalyst over the monolith channels resulted in a good dispersion of catalysts over the cordierite surface. The mesoporous and uniform nanoparticles of TiO<sub>2</sub>, N/TiO<sub>2</sub> and Cu/TiO<sub>2</sub> could be seen in Fig. 2(d-f), respectively. Fig. 2(g-i) shows the elemental mapping images of pure TiO<sub>2</sub>, N/TiO<sub>2</sub> and Cu/TiO<sub>2</sub> samples. Noticeably, N and Cu metals, evenly distributed over the TiO<sub>2</sub> surface, can provide more active sites for the reactants. The EDX plots in Fig. 2(k-l) further confirmed the presence of N and Cu metals in TiO<sub>2</sub>.

The  $N_2$  adsorption-desorption tests were performed to determine the surface area, pore volume and pore width of the catalysts. The isotherms of TiO<sub>2</sub>, N/TiO<sub>2</sub> and Cu/TiO<sub>2</sub> samples are illustrated in Fig. 3. Evidently, all the samples exhibited typical type IV isotherms

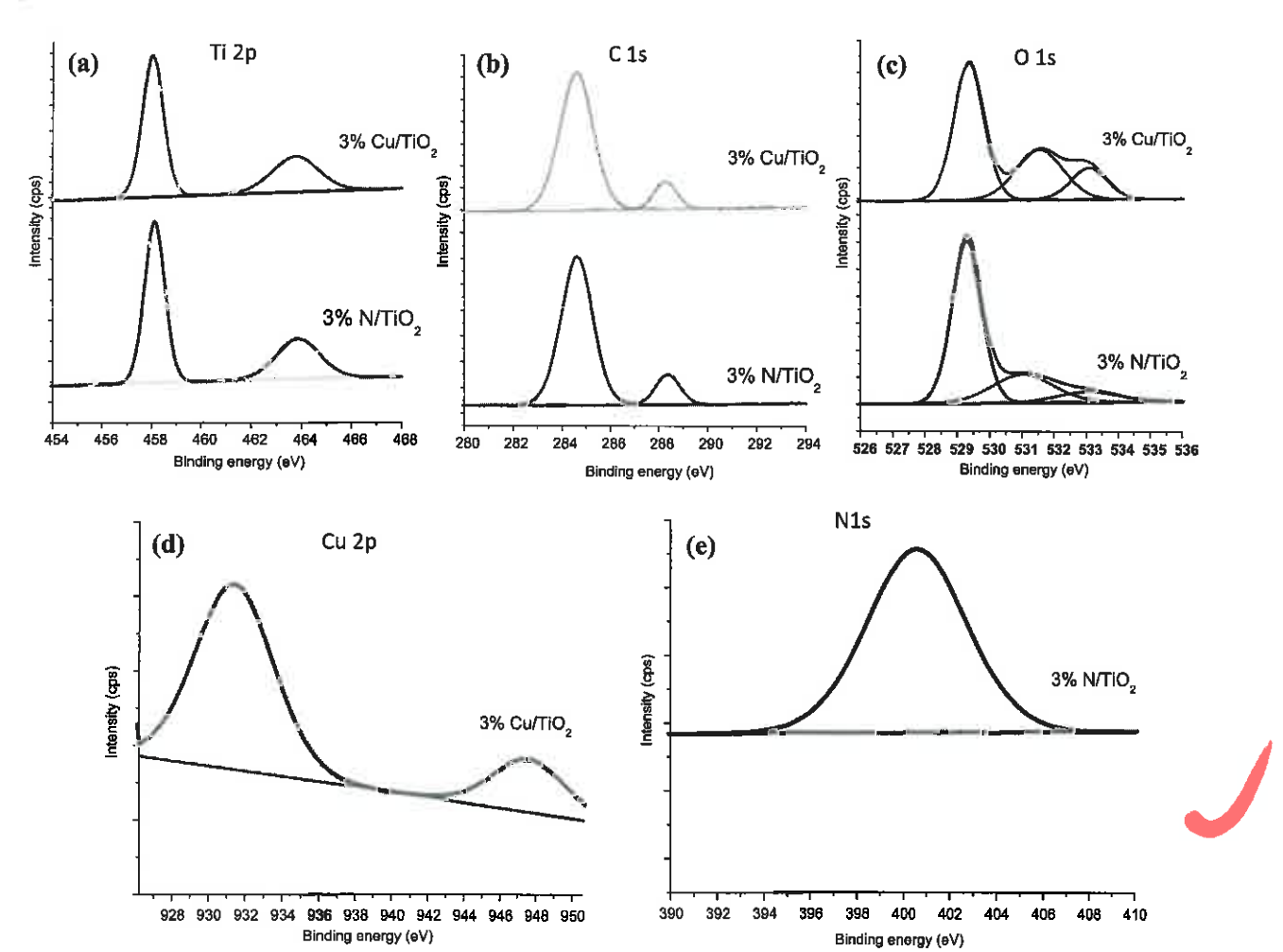


Fig. 4. XPS spectra of 3% N/TiO<sub>2</sub> and 3% Cu/TiO<sub>2</sub> samples: (a) Ti2p spectra of N/TiO<sub>2</sub> and Cu/TiO<sub>2</sub>, (b-c) O1s and C1s spectra of N/TiO<sub>2</sub> and Cu/TiO<sub>2</sub> samples, (d) Cu2p spectra of Cu/TiO<sub>2</sub> and (e) N1s spectra of N/TiO<sub>2</sub>.

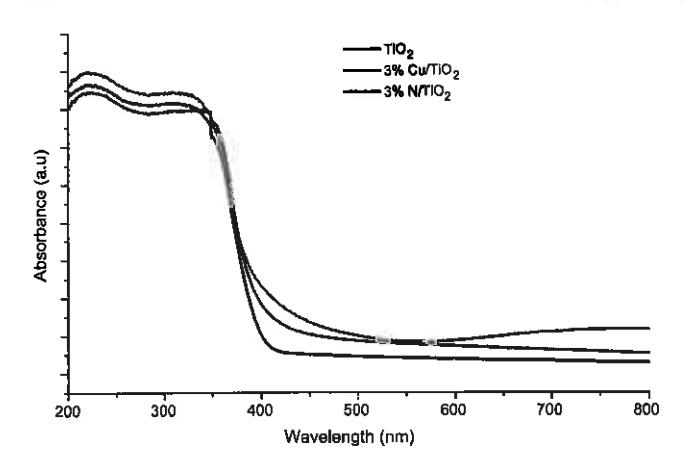


Fig. 5. UV–vis diffuse reflectance absorbance spectra of  $TiO_2$  and doped  $TiO_2$  samples.

with an increase in the volume of gas uptake. The hysteresis loops observed in all the samples, indicating mesoporous pore structure of TiO<sub>2</sub>. Suggestively, capillary and condensation reflections were observed in the TiO<sub>2</sub> sample, while the similar trends appeared in the N and Cu doped TiO<sub>2</sub> samples. BET surface area was measured from N<sub>2</sub> adsorption-desorption isotherms and the results are listed in Table 1. The BET surface area of TiO<sub>2</sub> was 42 increased to 47 and 50 m<sup>2</sup>/g in N/TiO<sub>2</sub> and Cu/TiO<sub>2</sub> samples, respectively. It is noticeable to see there is no significant effect on TiO<sub>2</sub> surface area by loading Cu and N metals. However, pore volume gradually increased with Cu and N loading.

X-ray photoelectron spectroscopy (XPS) was used to determine the oxidation state of Ti, and chemical states of the component elements in 3 wt.% N/TiO2 and 3 wt.% Cu/TiO2 samples as presented in Fig. 4. The Ti  $2p_{3/2}$  and Ti  $2p_{1/2}$  binding energies (BE) in Fig. 4(a) attributed to the presence of titanium as Ti4+ oxidation state in both N/TiO2 and Cu/TiO2 samples. Fig. 4(b) shows spectra of O1s for the N/TiO2 and Cu/TiO2 samples. The XPS spectrum of O1s in N/TiO2 reveals a peak with main components, one at 529.37 eV, characteristics of lattice oxygen (O2-) and a high bending energy component at 531.57 and 533.11 eV related to metal-OH bond or free hydroxyl group (OH) on the surface. The same kind of analysis fitting can be determined for Cu/TiO2 sample. The C1s peaks for N/TiO2 and Cu/TiO2 samples are presented in Fig. 4(c). The main peak at 284.60 eV is assigned to C-C and C-H hydrocarbon bonds. The peak at 288.31 eV can be attributed to carbon atoms bound to oxygen with double bond C=O. The relative concentration of peak at 284.60 eV was much more and may be recognized as the carbon from carbon tap used for sample analysis. Fig. 4(d) shows the spectra of Cu 2p peaks for Cu/TiO2 with BE regions centered at  $\sim$  931.41 eV (2p3/2 and 947.48 eV (2p1/2), respectively, indicating copper as Cu2+ or copper oxide (CuO) [34]. Fig. 4(e) shows spectrum of N/TiO2 contains N 1s peak at approximately 400 eV, which reflects a chemical structure like O-Ti-N [2].

Fig. 5 shows UV-vis diffuse reflectance absorbance spectra of pure TiO<sub>2</sub>, N/TiO<sub>2</sub> and Cu/TiO<sub>2</sub> catalysts. The addition of N and Cu can obviously enhance the absorbance of TiO<sub>2</sub> under visible light irradiations. The band gap energy was measured from a plot of  $(\alpha hv)^2$  versus (hv) using the direct method and the results are presented in Table 1. The band gap energy of TiO<sub>2</sub> shifted towards the visible region by doping with Cu and N which is in good agreement with previous reports [23,35].

The photoluminescence (PL) spectra of  $TiO_2$ ,  $N/TiO_2$  and  $Cu/TiO_2$  samples are displayed in Fig. 6. The fluorescence peaks of  $TiO_2$  and doped  $TiO_2$  samples were in the range of  $450-550\,\mathrm{nm}$  excited at wavelength  $350\,\mathrm{nm}$ . The pure  $TiO_2$  and doped  $TiO_2$  peaks exhibited

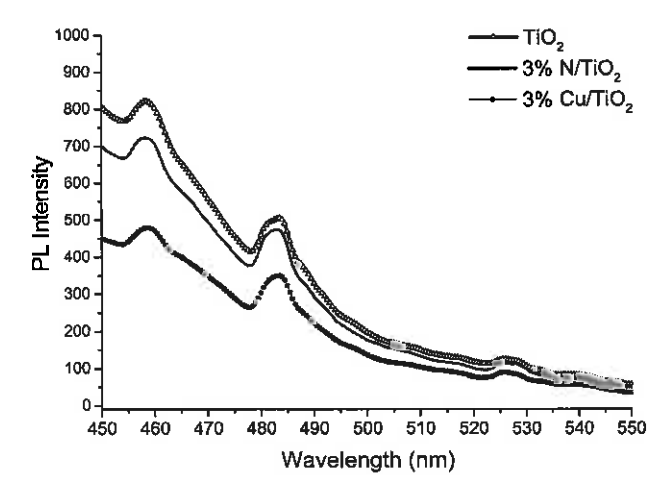


Fig. 6. Photoluminescence (PL) emission spectra of TiO<sub>2</sub> and Cu/N doped TiO<sub>2</sub> samples under the excitation wavelength of 350 nm.

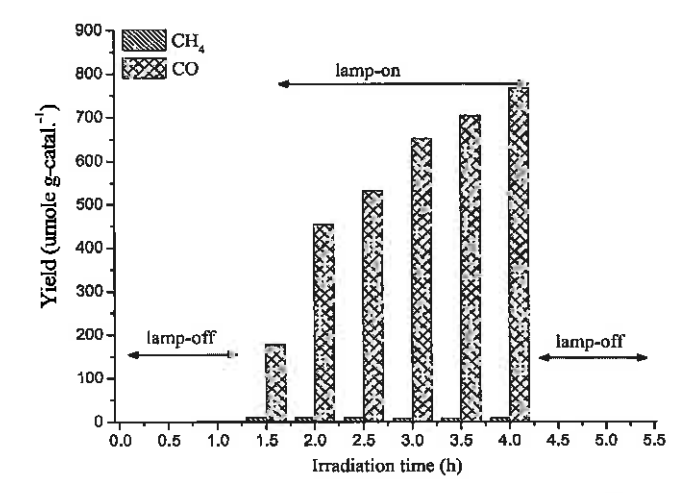


Fig. 7. Preliminary analysis of cordierite honeycomb loaded photocatalyst for  $CO_2$  reduction with  $H_2$  to CO and  $CH_4$  under the lamp off and on condition in a continuous operation of photoreactor.

wide and strong PL signals in the identical regions. The existence of PL attributed to the recombination of  $e^-/h^+$  pairs. In N/TiO<sub>2</sub>, lower PL intensities compare to pure TiO<sub>2</sub>, confirming hindered charges recombination rates by N. However, a significant decrease in PL intensity detected in Cu/TiO<sub>2</sub> sample probably Cu traps more electrons, thus prevents efficient charges recombination rate compared to N/TiO<sub>2</sub> and pure TiO<sub>2</sub> samples. Thus, it is anticipated that Cu would be more efficient than N to enhance TiO<sub>2</sub> photoactivity.

#### 3.2. Photocatalytic CO2 reduction with H2

The control experiments were conducted for  $CO_2$  reduction with  $H_2$  under UV light irradiation at  $100\,^{\circ}$ C,  $CO_2/H_2$  ratio 1.0 and feed flow rate  $20\,\text{mL/min}$ . In all the experiments carbon containing compounds were not detected in the reaction system when the lamp was off as shown in Fig. 7. However, a continuous CO and  $CH_4$  production could be seen under light irradiation. This confirmed that the catalysts and monoliths were cleaned while carbon containing compounds were produced from  $CO_2$  reduction only.

The effect of N-doping into TiO<sub>2</sub> photoactivity for CO<sub>2</sub> photoreduction with H<sub>2</sub> to CO and CH<sub>4</sub> under UV-light irradiation in a continuous monolith photoreactor is depicted in Fig. 8(a). CO was detected as the major CO<sub>2</sub> reduction product with a smaller

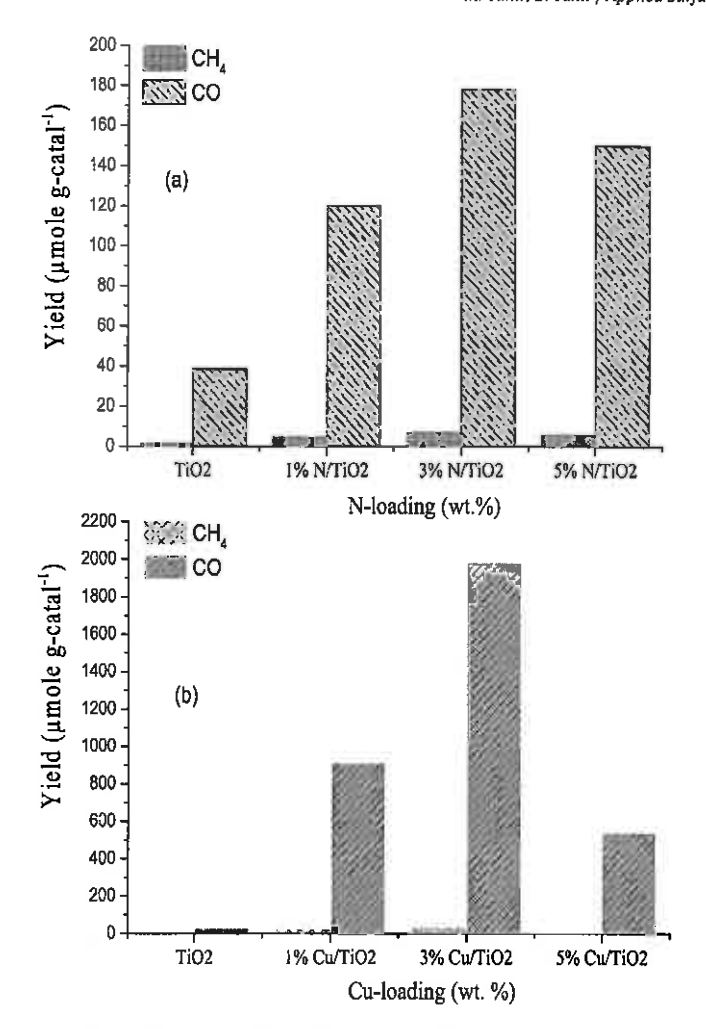


Fig. 8. Effect of N and Cu loading on  $TiO_2$  photoactivity for dynamic  $CO_2$  reduction to CO and  $CH_4$  in a continuous operation photoreactor at  $CO_2/H_2$  ratio 1.0 and feed flow rate 20 mL/min; (a) effect of N-loading, (b) effect of Cu-loading.

amount of CH<sub>4</sub> over both un-doped TiO<sub>2</sub> and N/TiO<sub>2</sub> samples. Pure TiO<sub>2</sub> scarcely reduced CO<sub>2</sub> and showed very poor activity for CO formation, but loading N enhanced CO production rate. The CO evolution increased remarkably with increasing N-doping up to an optimum and then gradually decreased. The large quantity of N-doping would result in more defect sites resulting in decreased photocatalytic activity [23]. Owing to the overall effects of defect sites, 3 wt.% N is an optimum amount to achieve the best photocatalytic activity in the present system.

Fig. 8(b) shows the effect of different amounts of Cu-loading (1 wt.%, 3 wt.% and 5 wt.% Cu contents) on the TiO2 photoactivity for dynamic CO2 conversion with H2 under UV light irradiation. In all the cases, CO was the main product during CO2 photoreduction with the smaller amount of CH4. Noticeably, Cu-loading can increase CO2 reduction efficiency for both CO and CH4 production. In the presence of a small amount of Cu-content (1 wt.%), the photoactivity of TiO2 was obviously enhanced. The activity of TiO<sub>2</sub> sample was further improved with increasing Cu-loading to 3 wt.% and the amount of CO detected was 1981 µmole g-catal. -1. This yield of CO production was higher than that of pure TiO2 by more than 99 times. When Cu-loading was more than 5 wt.%, a reduction of photoactivity was observed. This was probably due to loading of excess Cu over the TiO<sub>2</sub> surface (shielding effect), causing a decrease of TiO2 surface active sites or perhaps due to recombination centers over the TiO2 surface [4,32]. Therefore, 3 wt.%

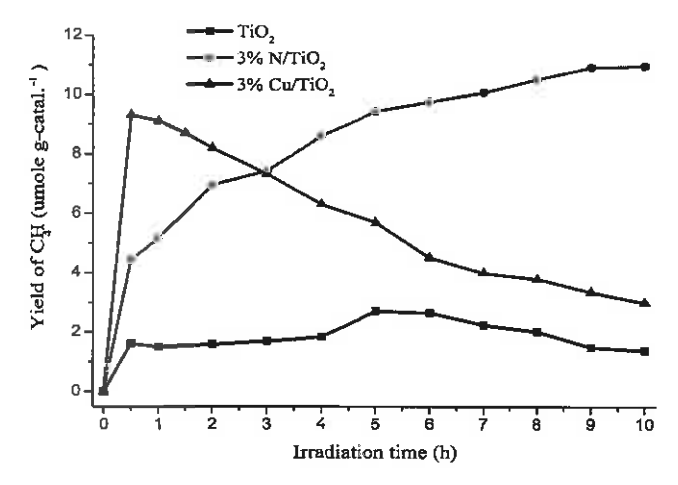


Fig. 9. Effect of irradiation time on  $CC_2$  photoreduction with  $H_2$  to  $CH_4$  over  $TiO_2$  and doped  $TiO_2$  catalysts in continuous monolith photoreactor at  $CO_2/H_2$  ratio 1.0 and the feed flow rate 20 mL/min.

Cu/TiO<sub>2</sub> has the highest activity over which maximum CO yield observed, considerably more than the amount of CO produced over N/TiO<sub>2</sub> and TiO<sub>2</sub> catalysts, This enhancement in the Cu/TiO<sub>2</sub> activity for CO production was probably due to the higher mobility of charges with hindered recombination rate by Cu-metal in monolith microchannels. Hence, Cu-metal has more ability to trap electrons as evidenced by PL analysis and due to the reduction potential difference of Cu/TiO<sub>2</sub> system, resulting in enhanced productivity [3].

Further investigations were carried out to study the effect of irradiation time on dynamic photocatalytic CO2 reduction in a continuous photoreactor operation. Fig. 9 presents a dynamic CH<sub>4</sub> production over Cu/TiO2 and N/TiO2 catalysts at different irradiation time. Noticeably, Cu and N metals have different effects on CH<sub>4</sub> production. Increasing formation of CH<sub>4</sub> was observed over the N/TiO2 catalyst during the entire irradiation time. CH4 formation over Cu/TiO<sub>2</sub> presented a different behavior, initially reaching maximum concentration, and then gradually decreased. The decreased in CH<sub>4</sub> production over the irradiation time was possibly due to oxidation of CH4 with O2 to CO2 in the presence of an efficient Cu/TiO2 monolithic catalyst [36]. On the other hand, N enables trapping holes, resulting in a continual increase in the yield rate of CH<sub>4</sub>. This also revealed prolonged stability and efficiency of N/TiO<sub>2</sub> catalyst for dynamic CH4 production in a continuous operation of photoreactor [23].

Previously, it has been reported that both Cu and N doped TiO2 photocatalysts could enhance CH4 photo-generation over the irradiation time. We investigated continuous CH4 and hydrocarbon production over a Cu-In/TiO2 catalyst in a batch mode operation of monolith photoreactor under UV-light irradiation [4]. Liu et al. [37] reported increased in CH4 yield rate with the irradiation time using Cu/TiO2 catalysts in a slurry type photoreactor system. However, in the current study, different trends in CH4 production over the cordierite honeycombs were perhaps due to gas phase reaction in a continuous monolith photoreactor operation. Similarly, Li et al. [23] observed CH<sub>4</sub> evolution rate increased with the irradiation time over N/TiO2 during gas phase CO2 reduction in a batch photoreactor under visible light irradiation. In this case CH<sub>4</sub> production trends are similar to current results, confirming N loading helps to produce CH4 both in the gas phase and continuous operation of photoreactor. This also confirms higher stability and activity of N/TiO2 for dynamic CH4 production.

The yield of CO production during CO<sub>2</sub> reduction over TiO<sub>2</sub> and doped TiO<sub>2</sub> samples at different irradiation times is presented in

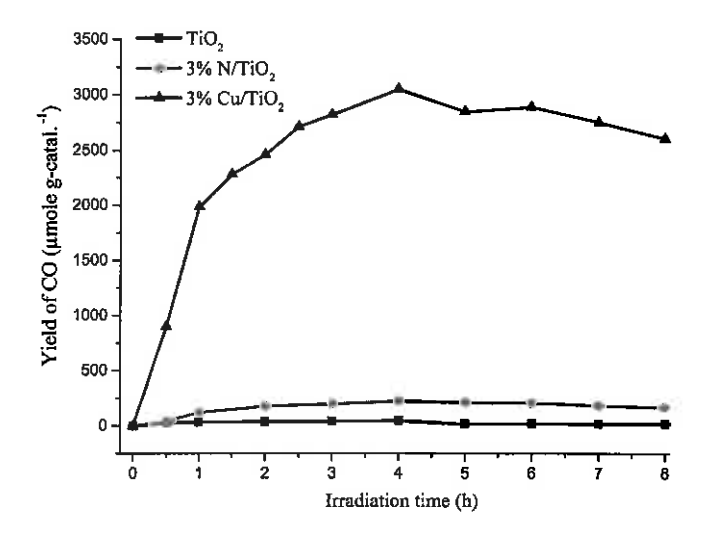


Fig. 10. Production of CO during  $CO_2$  reduction with  $H_2$  over  $TiO_2$  and modified  $TiO_2$  samples in continuous monolith photoreactor at  $CO_2/H_2$  ratio 1.0 and the feed flow rate 20 mL/min.

Fig. 10. Initially, the yield of CO production is much faster, but gradually decreased after 4h of irradiation time. However, the amount of CO over a  $\text{Cu/TiO}_2$  monolithic catalyst was significantly higher than N/TiO<sub>2</sub> and pure  $\text{TiO}_2$ . The much higher photoactivity for CO production confirms the potential of  $\text{CO}_2$  reduction with  $\text{H}_2$  in a continuous operation of photoreactor loaded with  $\text{Cu/TiO}_2$  nanoparticles. However, the CO production rate was gradually decreased at a prolonged irradiation time due to oxidation of CO to  $\text{CO}_2$  in the presence of  $\text{O}_2$  or perhaps due to deteriorating catalysts photoactivity in the course of continuous  $\text{CO}_2$  reduction over the irradiation time [31,36].

Table 1 summarizes yield rates and selectivity of different products over TiO<sub>2</sub> and doped TiO<sub>2</sub> catalysts. The main products observed were CO and CH<sub>4</sub> over TiO<sub>2</sub> and doped TiO<sub>2</sub> monolithic catalysts. However, in the case of Cu/TiO<sub>2</sub>, smaller amount of hydrocarbons namely C<sub>2</sub>H<sub>4</sub>, C<sub>2</sub>H<sub>6</sub>, C<sub>3</sub>H<sub>6</sub> and C<sub>3</sub>H<sub>8</sub> were also detected in the gas mixture. The performance of Cu/TiO<sub>2</sub> was found to be the highest, giving a dynamic CO yield rate of 763  $\mu$ mole g-catal.  $^{-1}$  h  $^{-1}$  a 14 fold more efficient than N/TiO<sub>2</sub> and 64 times more CO production over copper than un-doped TiO<sub>2</sub> catalyst. The selectivity of CO production over TiO<sub>2</sub> and N/TiO<sub>2</sub> were much closer (96%) but increased to 99% in Cu/TiO<sub>2</sub> catalyst. However, the production of CO as the main product over Cu/TiO<sub>2</sub> and N/TiO<sub>2</sub> was due to thermodynamic reduction potential difference between TiO<sub>2</sub> (-0.5 eV) and CO<sub>2</sub>/CO (-0.48 eV) [2].

Photocatalytic CO<sub>2</sub> reduction by H<sub>2</sub> via reverse water gas shift (RWGS) reaction also contributed to CO production. Recently, it has been reported that CO<sub>2</sub> was firstly converted to CO and then transformed to CH<sub>4</sub> over TiO<sub>2</sub> based photocatalysts [38,39]. However, in the present study, due to continuous operation of photoreactor and efficient adsorption-desorption process inside monolith microchannels, CO was dynamically removed from the reactor over the irradiation time. Previously, we have investigated photocatalytic CO<sub>2</sub> reduction to CO over different co-doped TiO<sub>2</sub> nanocatalysts in a batch mode of monolith photoreactor. [4,30,31,39–41]. Therefore, it can be established that CO would be a major CO<sub>2</sub> reduction product via RWGS reaction in a monolith photoreactor operated in a batch or continuous mode of operation.

From Table 1, it is obvious that surface area, crystal size and band gap energy of Cu/TiO<sub>2</sub> and N/TiO<sub>2</sub> are much closer to each other. The higher Cu/TiO<sub>2</sub> photoactivity could not be linked to surface area or band gap energy. Therefore, enhanced Cu/TiO<sub>2</sub> photoactivity could

be due to higher mobility of electrons in Cu-doped  $TiO_2$  samples as illustrated in Eqs. (1)-(3) [4,42].

$$Cu^{0} + h^{\dagger} \rightarrow Cu^{\dagger} + e^{-} \tag{1}$$

$$Cu^{+} + h^{+} \rightarrow Cu^{2+} + e^{-}$$
 (2)

$$Cu^{+}/Cu^{2+} + e^{-}/2e^{-} \rightarrow Cu + h^{+}/2h^{+}$$
 (3)

The generation of Cu ions takes place through the oxidation of Cu metal by photo-generated holes (Eq. (1)). Due to rapid transfer of excited electrons to the Cu particles,  $e^-/h^+$  pair's separation is enhanced as illustrated in Eqs. (2) and (3). Therefore, role of Cu in  $CO_2$  reduction over  $Cu/TiO_2$  is noticeable. As a consequence, higher photoactivity could be seen over  $Cu/TiO_2$  monolithic photocatalyst for CO production. Recently, similar observations have been reported for photocatalytic  $CO_2$  reduction to CO and  $CH_4$  over  $Cu/TiO_2$  photocatalyst in a gas phase system [43].

In order to investigate the performance of CO<sub>2</sub> photoreduction with H2 over Cu and N doped TiO2 photocatalysts in a continuous monolith photoreactor, the results are compared with the work reported by various researchers. N/TiO2 catalyst was used for CH<sub>3</sub>OH production and yield rate of 23 μmole g-catal. -1 h-1 was measured using a batch mode photoreactor [22]. CO2 reduction with H<sub>2</sub>O to CO was reported over g-C<sub>3</sub>N<sub>4</sub>-N-TiO<sub>2</sub> in batch mode operation with a maximum yield of 14.73 µmole after 12 h irradiation time [44]. Over I/TiO2 and Cu-I/TiO2, a CO yield rate of 3.9 and 12 \(\mu\)mole g-catal. \(^{-1}\) was reported after 3.5 h during gas phase CO2 reduction in a batch mode operation [20]. Similarly, photocatalytic CO2 reduction with H2O to CH4 over different photocatalysts such as CH<sub>4</sub> yield of 100.22 ppm cm<sup>-2</sup> h<sup>-1</sup> over MgO/TNTs [45], 17 µmole g-catal.-1 of CH<sub>4</sub> yield after 7 h over Ca<sub>1.0</sub>Ti<sub>1.0</sub>O<sub>3</sub> [46], rGO-Pt/TNTs with CH<sub>4</sub> yield rate of 10.96  $\mu$ mole m<sup>-2</sup> [15], CH<sub>4</sub> yield rate of 23.10 µmole g-catal. 1 after 480 min over 3-D Au/TiO<sub>2</sub> nanoparticles [47] and a CH<sub>4</sub> production of 184 μmole gcatal.-1 after 24h over Zn-Cu promoted TiO2 has been reported by various researchers [38]. A comparison study between previous reports and current study revealed that monolith geometry facilitated in improving the photoactivity and selectivity of photocatalysts. Therefore, the role of cordierite honeycomb monolith loaded with Cu and N is obvious for dynamic CO production in continuous photoreactor operation. This is perceptibly due to a larger illuminated surface area with higher photon energy consumption inside the monolith channels [39].

The performance of cordierite honeycomb support loaded with Cu and N metals was further examined based on the quantum yield, calculated for each experiment, as the ratio of the product rate (mole per s) with photonic flux (mole per s). The quantum yield of CO<sub>2</sub> photoreduction to CO can be defined as the ratio of production rate (mole per s) with photonic flux (mole per s) as shown in Eq. (4) [48].

Quantum yield of CO(%)

$$= \frac{2 \times \text{moles of CO production rate(mol/sec)}}{\text{moles of photon flux(mol/sec)}} \times 100$$
 (4)

The quantum yield was calculated based on the CO production rate and moles of photon input energy over the catalyst surface as presented in Table 1. The quantum yield for dynamic CO production over cordierite honeycomb monoliths loaded with  $Cu/TiO_2$  was greatly enhanced (0.083%) than  $N/TiO_2$  and  $TiO_2$  samples. Liou et al. [26] reported quantum efficiency of 0.012% and 0.057% for methanol and acetaldehyde, respectively, during photocatalytic  $CO_2$  reduction with  $H_2O$  over  $NiO/InTaO_2$  catalysts in an internally illuminated continuous monolith photoreactor. Obviously, higher quantum yield in the current study was due to a larger illuminated surface area because of monolith microchannels and using  $H_2$  as a reductant.

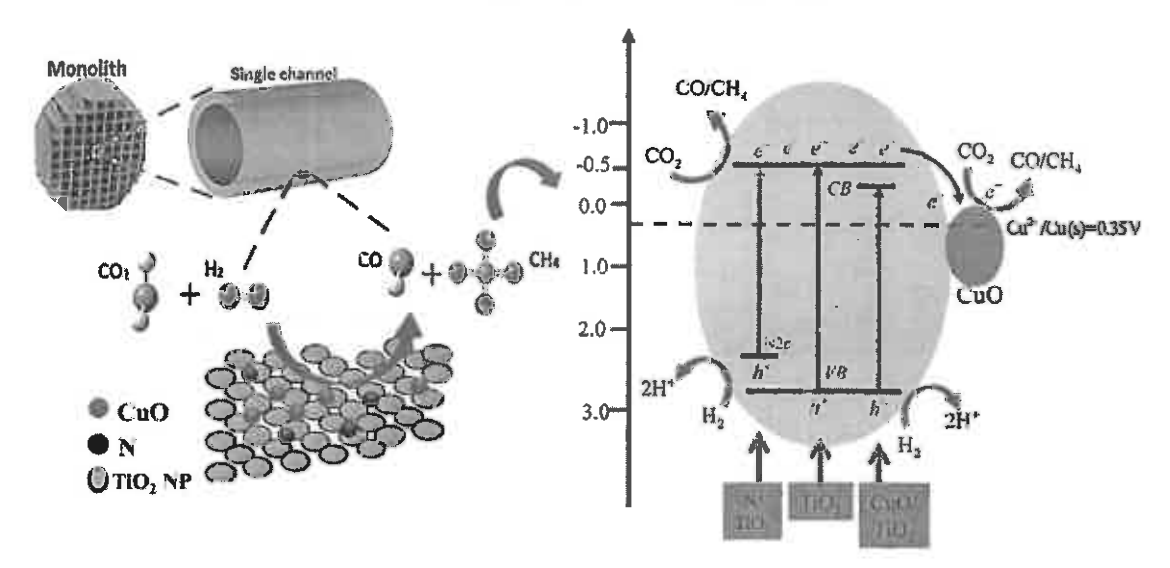


Fig. 11. Schematic of photocatalytic CO<sub>2</sub> reduction with H<sub>2</sub> over cordierite honeycomb loaded Cu/TiO<sub>2</sub> and N/TiO<sub>2</sub> catalysts.

#### 3.3. Reaction mechanism

In the photocatalytic  $CO_2$  reduction process, photo-generated electrons (e<sup>-</sup>) and holes (h<sup>+</sup>) involve in breaking O—C—O and H—H bonds with the formation of C—O and C—H bonds. The reaction mechanism was studied to get insight of  $CO_2$  photoreduction over  $Cu/TiO_2$  and  $N/TiO_2$  catalysts. The electron-hole pairs separation and production of  $CO_3$  and  $CO_4$  are illustrated in Eqs. (5)–(10) [42,43,49].

$$TiO_2 + hv \rightarrow h_{vh}^+ + e_{ch}^- \tag{5}$$

$$Cu^{2+} + 2e_{ch}^{-} \rightarrow Cu^{2+} - 2e_{ch}^{-}$$
 (6)

$$CO_2 + e_{cb}^{-} \rightarrow CO_2^{-} \tag{7}$$

$$H_2 + h_{\nu b}^+ \to H^+ + H^+$$
 (8)

$$CO_2 + 2H^+ + 2e^- \rightarrow CO + H_2O$$
 (9)

$$CO_2 + 8H^+ + 8e^- \rightarrow CH_4 + 2H_2O$$
 (10)

As the photocatalytic activity is closely related to the band structure of photocatalysts, separation and transportation of photogenerated carriers (i.e., electrons and holes) as well as the redox potential, the enhanced photocatalytic mechanism can be explained by the scheme presented in Fig. 11 [43,50]. Under the light irradiations, VB electrons of TiO2 excited to CB creating holes in VB. Without metals-loading, these charges recombine back and only a fraction of electrons and holes participate in reduction and oxidation process, thus, TiO2 shows a quite low photocatalytic activity. When Cu metal was loaded on TiO2 surface, the CB electron of TiO<sub>2</sub> can transfer to these metals which cause electron-hole pair separation (Eq. (6)). Furthermore, more electrons could be trapped if the metal reduction potential is more positive than the CB of TiO2. As the redox value of Cu is lower (+0.35) than the CB of TiO2 (-0.50 V), thus electron can effectively be transferred to copper to prolong their lifetime [4,51,52], H<sub>2</sub> molecules were dissociated to H<sup>+</sup> ions while CO<sub>2</sub> reduced to CO and hydrocarbons by accepting the trapped electrons and H+ ions as explained in Eqs. (7)-(10). Some previous works have reported that all of the N/TiO2 contributed to the visible light absorption by creating a new N 2p state slightly above the valence band of TiO2 [23]. As to the current N/TiO2 photocatalyst, upon UV-light irradiation, holes may be trapped by N to react with CO to produce CH4.

The expressively enhanced in CO yield rate over Cu/TiO $_2$  was clearly due to higher trapping and mobility of electrons by Cu metal for CO $_2$  reduction inside monolith channels. On the other hand, continuous production of CH $_4$  over N/TiO $_2$  was perhaps due to adsorbed CO converted to CH $_4$  over N/TiO $_2$  in the presence of holes. In general, dynamic CO $_2$  conversion to CO and CH $_4$  at a higher yield rate was due to using cordierite honeycomb monolith support loaded with doped TiO $_2$  nanoparticles.

#### 4. Conclusions

In this study, cordierite honeycombs loaded Cu/TiO2 and N/TiO2 nanocatalysts were developed for dynamic photocatalytic CO2 conversion with H2 under UV-light irradiation in a continuous operation monolith photoreactor. CO was the major CO2 reduction product with a smaller amount of CH4 over Cu and N/TiO2 catalysts. Cu could improve TiO2 photocatalytic activity by trapping electrons while N prolonged the lifetime of photo-generated charges by trapping holes. N-loading also promoted the formation of CH<sub>4</sub> during dynamic CO<sub>2</sub> reduction. The performance of Cu/TiO2 was found to be the highest, giving a CO yield rate of 763  $\mu$ mole g-catal.  $^{-1}$  h  $^{-1}$  a 14 fold more efficient than N/TiO2 and 64 times more than un-doped TiO<sub>2</sub> catalyst. The photoactivity of Cu and N/TiO2 samples gradually reduced after 4h of irradiation time. However, N/TiO2 found very stable for CH4 production over the entire irradiation time. In summary, by means of Cu and N doping, highest efficiency for dynamic CO2 conversion was obtained due to a larger illuminated surface area, higher photon energy and better charges separation inside monolith microchannels. Both Cu and N are equally important to exert a substantial impact on the enhancement of CO and CH4 production. This development confirmed a high performance of cordierite honeycomb monolith loaded with Cu/TiO2 than N/TiO2 for dynamic CO2 conversion to fuels.

#### Acknowledgement

The authors would like to extend their deepest appreciation to Universiti Teknologi Malaysia (UTM), Malaysia, for financial support of this research project under PAS RUG (Potential Academic Staff Research University Grant, Vot 02k24).

#### References

- [1] L. Yuan, Y.J. Xu, Photocatalytic conversion of CO<sub>2</sub> into value-added and renevable fuels, Appl. Surf. Sci. 342 (2015) 154-167.
- [2] Z.G. Zhang, Z.F. Hitang, X.D. Chang, O.L. Wang, Y. Chen, P.M. Dours, X.W. Zirang, Product selectivity of visible-light photocatalytic reduction of earlier dioxide using titanium dioxide deped by different nitrogen-sources, Appl. Surf. Sci. 350 (2015) 40-51.
- [3] M. Falsis, F.S. Amin, Indium-doped TiO<sub>2</sub> nanoparticles for photocatalytic CO<sub>2</sub> reduction with H-O vapous to CM<sub>2</sub>, Appl. Cutal. B: Environ. 162 (2015) 98–109. [4] 36. Tahir, R.S. Amin, Photocatalytic CO<sub>2</sub> reduction with H<sub>2</sub> as reduction over
- copper and indium co-doped TiO in mocatalysts in a monolity photore after, Appl, Catal. A: Gen. 493 (2015) 90-102.
- [5] H. Ahmed, Y. Shib, f., T. Taniguchi, Y. Izumi, Photocatalytic conversion of carbon dioxide into methanol using zinc-copper-M(III) (M- aluminuta, nallium) layered double hydroxidos, J. Catal. 270 (2011) 123–135.
- M. Jahli, H.S. Amin, Photocately the reduction of carbon dioxide with twice vapors over mont noriflonite modified TiQ+ napocomposites, Appl. Catif. 6:
- Environ. 142–145 (2013) 512–522. [7] J. Ye, R. Wang, M.Z. Wu, Y.P. Yuan, A review on g-C<sub>3</sub>N<sub>2</sub> io. photocatalytic water splitting and CO<sub>2</sub> reduction. Appl. Surf. Sci. 258 (2015) 15–27.
- [8] J. Low, J. Yu, W. Ho, Graphens-based photocatalysts for CO\_reduction to solar fuel, J. Phys., Chem. Lett. 6 (2010) 4244-4251.
   [9] J. Yu, J. Low, W. Xiao, P. Zhou, M. Jaroniac, Enhanced photocatalytic
- CO--: duction activity of anatase TiO2 by courposed (001) and [101] facutt, J.
- Am, Cheric God. 139 (2014) 8339-8842. [10] R. Sasikata, A.R. Shirole, V. Sudarsan, Jagannath, C. Sudakar, R. Naik, R. Fuo, S.R. Bharadwaj, Enhanced photocatalytic activity of indium and chrogen co-depert 750-01'd nanonomposites for hydrogen generation, Appl. Catal. As Gen. 377 (1.010) 47-34.
- [11] LJ. Liu, F. Gao, H.L. Zhao, Y. Li, Tailoring Cu valence and oxygen vacuus y in  $Cu/TiU_2$  entalys is for anhanced  $CO_2$  photoreduction efficiency, Appl. Catal. Is: Entiron, 134 (2015) 149-358.
- [12] D. Kong, J.Z.Y. Tin, F. Yang, J.L. Zyng, X.W. Zhang, Electrodeposited Agnaxogarticles on TiO<sub>2</sub> near one is for enhanced UV virible light photore juction CO<sub>2</sub> to CH<sub>2</sub>, Appl. Surf. Sci. 277 (2013) 105–119.
  [13] B.J. Tweel, R. Wigner L. K.-R. Park, H.-J. Ryu, J.-J. Back, M. Keng, Wethang
- icantalon are a photoreduction of CO2 with water using TiO2 includio. Wi
- remedient are a photogramming of CO<sub>2</sub> with water using TiO<sub>2</sub> including follogramming and the properties of CO<sub>2</sub> and the Aranga C. Zhong Zhong
- [16] Jii, Li, D.L. Leo, C.J. Viene, S.M. Fee, S.C. Chen, J.W. Lin, L. Zhu, K. Li, Copporally industrible francovaria an highly efficient photocatalysts for reduction of Control methanol and a visible light invadiation, J. Solid State Chem. 203 1.013, 154-151,
- [17] P.C. Li, J.F. Zu, H. Jing, C.X. Wu, H. Peng, J. Lu, H.Z. Yin, Wedged N-doped CuO with more magnifive conductive band and lower overpotential for high efficiency propodestric converting CO- to mer land, Appl. C. tal. B. Environ. 106 (2014) 124-140.
- [18] E.Z. Lin, L.L. Qi, J.J. Bian, Y.H. Chen, J. V. Hu, J. Fun, H.C. Liu, L.J. Zim, Q.P. Williag, In facility is a case to fabricate pharmonic Cu modified TiO $_2$  mass-flower films for pla for reduction of CO $_2$  to methanol. Mater. Res. Bull. 62 (2015) In 5–209.
- [19] J.V. Wang, G.E. Ji, Y.S. Liu, M.J. Gondell, X.F. Chang, Cu-OpilOp Teterostructure man fully arrays prepared by an electrodeposition method exhibiting anhanced photocatalytic activity for CO<sub>2</sub> reduction to methanol, Catal. Commun. 45 (2014) 17-21.
- [20] G. Zhane, T. Cao, J.M. Andino, Y. Di, Copper and Leding co-modified TiO2 nanaparticles for improved and dty of COs photocolaction with water vapor, Appl. Cos. J. B. Environ. 125-134 (2012) 257-264.

  [21] H.Y. Yin, Z.L. Wang, L. Wang, G.L. Nie, Y. Zheng, W.W. Wu, Cos. O. TiO<sub>2</sub>.
- [21] First the Adversity of the
- TiU2-nitrogen modifical photocatulyst, J. Cu2 Util. 5 (2014) 47-52.
- [23] X. Li, Z. Zhuru, z. W. Li, H. Pan, Photocatalytic reduction of CO2 over noble actal-linded and nitrogen-doped metoporous iiiO\_, Appl. Catal. A: Gen. 429-130 (2012) 31-35.
- [24] O. Ola, E.M. Muroto-Valor, Review of material design and reactor engineering on the photoc delysis for CO, reduction, J. Phatochem. Photobiol. C
- Pilotrickern, Rev. 24 (2015) 16–42. [25] R.Z. de Fichler, T.Z. Mires, S. Caillol, Pichting global warming by photocaraly de-reduction of CO<sub>2</sub> using glant photocatalytic reactors. Renew, Surtain, Energy Rev. 10 (2011) 52-100

- [26] P.Y. Liou, S.C. Chen, J.C.S. Wu, D. Liu, S. Mackintosh, M. Maroto-Valer, R. Linforth, Photocatalytic CO<sub>2</sub> reduction using an internally illuminated
- monodith photorcactor, Energy Environ. Sci. 4 (2011) 1487–1494.

  [27] E. Tabolda, I. Angurall, J. Liuma, Hydrogen photoproduction from bio-derived alrehole in an optical abor honeycomb reactor loaded with Ar/TiO2, 1.
- Photochem. Thorobiol. A: Chem. 261 (2014) 35–39.

  [28] K. Yuan, L. Yang, X. Du, Y. Yang, Performance analysis of photocatalysic COreduction in optical fiber monolith reactor with multiple inverse lights. Energy Convers. Manage, 81 (2014) 98-105.
- [29] T. Beenich, T. Muhammad, A. Noraishah Saidina, Photoreactor cartion dioxide reduction with hydrogen in a continuous catelytic monulith photoreactor, Cheta, Engin, Trans. 45 (2015) 259–264.
- [30] B. Tahir, M. Talair, N.A.S. Amin, Gold-indium modified TiO2 nanocatalysts for photo catalytic CO2 reduction with He as reductant in a monolith photore actor, Appl. Surf. Sci. 338 (2015) 1-14.
- [31] M. Pakir, N.J. Amin. Forior nance analysis of nanostructured NiU-In-O-/110callely at for CO2 photory duction with He in a monolith photoreactor, Chem. Eng. J. 235 (2016) 655-649
- [32] F. Concli, A.V. Puga, B. Julián-López, H. García, A. Corma, Copper-doped titania photocetalysts for simultaneous reduction of CO2 and production of H2 from equeeus sulfide, Appl. Catal. B: Environ, 180 (2016) 263-270.
- M.S. Alipla, J.X. Low, Z.Y. Qin, S. Wageh, A.A. Al-Ghamdi, J.G. Yu. S.W. Liu, Nitrogen-doped TiO<sub>2</sub> microalteets with enhanced visible light photocatalytic activity for CO<sub>2</sub> reduction, Chin. J. Catal. 36 (2015) 2127–2134.

  [34] Zn-Cu promoted TiO<sub>2</sub> photocatalyst for CO<sub>2</sub> reduction with H2O under UV
- [35] J.Z.Y. Tan, Y. rc. nandez, D. Liu, M. Maroto-Valer, J.C. Bian, X.W. Zhang Photos: duction of CO<sub>2</sub> using coppen-decorated TiO<sub>2</sub> nanorod films with localized surface phomon behavior, Chem. Phys. Lett. **531** (2012) **149**–154.
- [36] A. Cybult, M. Kiein, A. Zaleika, M. thane formation over riCy-based
- photocatalysts: reaction pathways, Appl. Catal. B 164 (2015) 433–442.

  [37] D. Liu, Y. Fernández, O. Ola, S. Mackintosh, M. Maroto-Valer, C.M.A. Parlett, A.F. Lee, J.C.S. Wu, On the impact of Cu dispersion on CO<sub>2</sub> photoreduction over Cu, riO<sub>2</sub>, Catal. Commun. 25 (2012) 78-82.
- [38] P.M. Faulino, V.M.M. Salim, N.S. Resende, Zn-Cu promoted TiO₂ photocatalyst for CC -reduction with H-O under JV light, Appl. Catal. B: Environ. 155 (2016) 362-570.
- [39] S. Tahir, M. Tahir, A.S. Amin, Performance analysis of monothis photoreactor
- for  $CO_2$  reduction with  $E_3$ , Energy Convers, Manage, 90 (2015) 272–281. M. Takir, H. Takir, R.A.S. Amin, Gold-nanoparticle-modified  $TiO_2$  nanowires for plantium-subarsed photocatalytic  $CO_3$  reduction with  $H_2$  under visible light in Hilation, Appl. Surf. Sci. 356 (2015) 1289-1299.
- [41] M. Tahir, N.S. Amin, Firstocamilytic CO, reduction and kinetic mudy over In/Tit/2 mare particles supported microchannel monolith photoreactor, Appl. Catal. A: Gen. 467 (2013) 433–496.
- [42] C.H. Wang, X.T. Zhang, Y.C. Liu, Promotion of multi-electron transfer for
- [42] C.R. Wang, X.P. Zidang, T.C. Ed., Prohibition of inflate-electron transfer for cultimored photocutallysis: a review focused on oxygen reduction reaction, Appl. Surf. Sci. 378 (2015) 26-45.
  [43] S.R. Chen, V.H. Nguyen, J.C. Veu, R. Mertin, K. Koci, Production of renewable fuels by the photocytropenation of CO<sub>2</sub>: effect of the Cu species loaded onto TiO<sub>2</sub> photocatalysts, Phys. Chem. Chem. Phys. 15 (2016) 4942–4951.
- S. Zhou, Y. Liu, J.M. Li, Y.J. Wang, G.Y. Jiang, Z. Zhao, D.X. Wang, A.J. Duan, J. Liu, Y.C. Wei, Facile in situ synthesis of graphitic carbon nitride  $(g-C_3N_4)$ -N-TiO<sub>2</sub> injury/praction as an efficient photocatalyst for the selective photoceduction of CO, to CO, Appl. Catal. P. Linviron, 158 (2014) 20-29.
- [45] C. Li, L. Zong, C. Li, J. Yang, Reprint of Photocatalytic reduction of CO<sub>2</sub> on MigO<sub>7</sub>TiO<sub>2</sub> nanotube films, Appl. Surf. Sci. 3.19 (2014) 16–20.
   [46] B.S. Kwalt, M. Kang, Photocatalytic reduction of CO<sub>2</sub> with H<sub>2</sub>O using
- perc milite CaxTiyO , Appl. Surf. Sci. 337 (2015) 138-144.
- J.Q. Jiao, Y.C. Wei, Z. Zhao, W.J. Zhong, J. Liu, J.M. Li, A.J. Duan, G.Y. Jiang, Synthesis of 3D ordered macroporous TiO2-supported Au nanoparticle photocatalysts and their photocatalytic performances for the reduction of  ${\rm CO}_2$  to meticane. Catal. Today 258 (2015) 319–326.
- [48] P. Di. J.T. Cameiro, J.A. Moulijn, G. Muí, A novel photocatalytic monclith reactor for multiplase i et rogeneous photocatalysis, Appl. Cat. I. A 334 (2008) 119-12%
- [49] C. Xilling, E. Chen, J. Yu. Graphene-based photocatalysts for solur-fuel cuer sion, Any, o. C.B in. Int. Ed. 04 (2015) 11250-11566.
- [50] O. Nu, J. Yu, J. Zhang, G. Liu, Cubic anatom TiO<sub>2</sub> nanocrystals with enhanced photocatalytic CO<sub>2</sub> reduction activity, Chem. Commun. 51 (2015) 7950–7953.
   [51] L. Li, E. Cheng, Y. Wang, J. Yu, Enhanced photocatalytic H<sub>2</sub>-production activity
- of bicor mone...t. (i')/riO2 composite nanofibers, J. Solid State Cher J. 449 (2015) 115-121.
- [52] 11. Planttion, E. Prilinima, S. Kotela, J. Guninzundi, Photocatalytic reduction of CO2 on copper-doped Titania catalysts prepared by improved-impregnation m-thod, C. tal. Commun. 6 (2005) 313-319.





Contents lists available at Science Direct

# Journal of Molecular Catalysis A: Chemical

journal homepage: www.elsevier.com/locate/molcata



# Highly efficient visible-light photocatalyst of nitrogen-doped TiO<sub>2</sub> nanoparticles sensitized by hematoporphyrin



Javad Saien, Zohreh Mesgari\*

Department of Applied Chemistry, Bu-Ali Sina University, Hamedan 65174, Iran

#### ARTICLE INFO

Article history:
Received 2 October 2015
Received in revised form
30 December 2015
Accepted 31 December 2015
Available online 6 January 2016

Keywords: Nitrogen doping Visible-light sensitizing Titania Hematoporphyrin Methyl orange

#### ABSTRACT

A novel hybrid nanocomposite based on N-doped TiO<sub>2</sub> nanoparticles was prepared and sensitized with hematoporphyrin for visible light utilization. The product was characterized by thermogravimetric analysis (TGA), different thermal analysis (DTA), X-ray diffraction (XRD), Fourier transform infrared spectroscopy (FT-IR), BET surface area analysis, UV-vis spectroscopy and field emission scanning electron microscopy (FE-SEM). The results showed that the N-doped TiO<sub>2</sub> has smaller crystalline size and larger specific surface area than bare TiO<sub>2</sub> particles. Surface oxygen defects, produced by nitrogen doping, would improve the advantage of hematoporphyrin placement and then facile electron exciting and transferring to the conduction band of N-doped TiO<sub>2</sub>. The crystal structure of N-doped TiO<sub>2</sub> was not affected by the sensitizing; however, the surface area was significantly increased. Application of the hybrid nanocomposite exhibited higher visible-light absorption leading to an enhancement of about 1.7 and 4.2 times in photocatalytic degradation of methyl orange compared with N-doped TiO<sub>2</sub> and just bare TiO<sub>2</sub> utilization, respectively. The photocatalytic degradation of methyl orange with the products was demonstrated to follow first order kinetic model. The produced nanocomposite can be reused at least four times recycling without significant loss of activity.

© 2016 Elsevier B.V. All rights reserved.

#### 1. Introduction

Today, the presence of injurious organic pollutants in wastewaters has caused serious environmental problems and thereupon purification of contaminated water is one fascinating challenge [1]. Accordingly, use of renewable energy has become an interesting research area because of its sustainability and positive effect on environment and the limited utilization of fossil fuels [2,3]. Solar energy, because of its great availability, its cleanliness as well as easy operation and use, has become the first choice in the field of renewable energy sources [4,5].

Another matter of interest is utilizing efficient and selective metal oxide semiconductors in the process of the photocatalytic degradation of organic pollutants [6,7]. A well-known semiconductor is TiO<sub>2</sub> with excellent photocatalytic properties that make it highly valuable for the oxidation of organic pollutants. It is a superior photocatalyst for both purification of water and air due to its nontoxicity, long-term stability, inexpensiveness and chemical stability over a wide pH range and also in a large number of solvents [3,9].

The sensitization of  $TiO_2$  by dyes such as ruthenium polypyridyl complexes [19], squaraines [20], porphyrins [21] and natural dyes [22] has been widely used for achieving desired electronic and

http://ducini.org/10.1010/f.nasicata.2013.12.027 1381-1169/© 2016 Elsevier B.V. All rights reserved.

One problem with pure TiO2 nanoparticle is its large band gap energy that can be activated under UV light irradiation. However, this situation limits its application under direct solar light, as UV light accounts for only a small fraction (<5%) of the solar spectra compared to visible region (45%) [10]. In order to eliminate this drawback and enhance the visible region absorption of TiO2, different approaches have been proposed in the literature. Since the discovery of activity of nitrogen-doped TiO2 under visible light irradiation by Asahi et al. [11], great attention has been given to doping TiO<sub>2</sub> by nitrogen atom [12-15]. Insertion of N atom produces a localized energy state above the valence band of TiO2, thus when N doped  $TiO_2$  is exposed to visible light, electrons are transferred from these localized states to the conduction band [16]. Compared to the other non-metal dopants (S, P and C), N-doped TiO2 materials represent a considerable photocatalytic activity and strong absorption under visible light irradiation [17,18]. Evidently, the mechanism of nitrogen doping to increase the visible-light absorption and photocatalytic activity of TiO2 is different from that of dye sensitization. It is therefore, concluded that coupling of nitrogen doping with dye sensitization is a good way to significantly improve the visible-light absorption and photocatalytic activity of TiO2.

<sup>\*</sup> Corresponding author. Fax: +98 81 38257407.

E-mail address: Linesgari91 Filesculatir (Z. Mesgari).

optical properties. As a surface modification technology, dye sensitization can solve two major drawbacks of ultrafast recombination of photogenerated electron-hole pairs and a low quantum yield [5]. Highly efficient dye sensitizers should meet the following needs: (i) a wide range of absorption spectrum, intense substrate adsorption capacity efficiency; (ii) high quantum yield and excited states with long lifetime; and (iii) matching band structure to decline energy loss during the process of electron transfer [23-25]. Porphyrin and porphyrin derivatives, because of their strong light absorption in the region of 400-450 nm (Soret band), as well as 500-700 nm (Q band), are appropriate candidates for sensitizing different structures of TiO2 semiconductors. One of porphyrin derivatives, hematoporphyrin (HP), is of natural origin derived from acid extraction of blood. The chemical structure of HP is similar to chlorophyll and the "hem" of hemoglobin, that are well known in nature [23]. HP consists of very large conjugated double bonds of tetrapyrrole, this extended conjugation leads to strong absorption of the visible spectrum with a thermal and photochemical stability. In this case, the sensitizer dye molecules bonded on the surface of TiO<sub>2</sub> can be excited by visible light and then the photoinduced electrons transfer into the conduction band (CB) of  ${\rm TiO_2}$  is facilitated. While CB injected electron reacts with acceptor molecules, i.e. with dissolved oxygen in solutions around TiO2 surface and forming  $O_2^{\bullet-}$  and HO $^{\bullet}$ ; the valence band (VB) remains unaffected [27,28]. The use of HP has been reported to meet the requirements relating to cost efficiency, non-toxicity and complete biodegradation.

In the present investigation, we present a novel hybrid nanocomposite, produced from N-doped TiO<sub>2</sub> nanoparticles and hematoporphyrin (HP/N-TiO<sub>2</sub>). Nanoparticles of N-doped TiO<sub>2</sub> (N-TiO<sub>2</sub>) are used as a matrix to prepare a dye-sensitized and visible-light active photocatalyst. The synthesized N-TiO<sub>2</sub> nanoparticles and the hybrid nanocomposite are then characterized by different techniques and the photocatalytic activity of the products are evaluated by the degradation rate of methyl orange (MO) as a model pollutant. Accordingly, the synergism effect of nitrogen doping and HP sensitizing is discussed.

#### 2. Experimental

#### 2.1. Materials

Sigma-Aldrich HP( $\geq$ 45%) was used without further purification. The tetraisopropyl-orthotitanate ( $\geq$ 98%), urea ( $\geq$ 99.5%), ethanol ( $\geq$ 99.9%), acetyl acetone ( $\geq$ 99.0%), mannitol ( $\geq$ 99.0%) and methyl orange (C.J. 13025) were purchased from Merck and used as received without any further purification. Fresh deionized water was prepared from a deionizer apparatus (Hastaran Co.) and used in the preparation of solutions.

#### 2.2. N-TiO<sub>2</sub> and HP/N-TiO<sub>2</sub> preparation

The nitrogen-doped titania, N-TiO<sub>2</sub>, product were prepared by the sol-gel method. For this aim, tetraisopropyl-orthotitanate (2.5 mL) was slowly added to a mixture of anhydrous ethanol (20 mL) and acetyl acetone (2.5 mL) with stirring at room temperature. Acetyl acetone was used as chelating agent to prevent precipitation of the tetraisopropyl-orthotitanate. After stirring for at least 60 min, the clear and yellow solution was obtained. We then added 3.0 mL dioionized water and stirred the mixture for 30 min. A few drop of concentrated HCl solution was then added to the sol to adjust the pH at about 1.7. At the next step, urea (4.0 g) was dissolved in ethanol and then added to the above solution. The mixture was stirred for 180 min at room temperature. The final solution was left overnight to form a wet gel. The wet gel was dried at 60°C and the resultant precipitate was ground in agate mortar. Finally

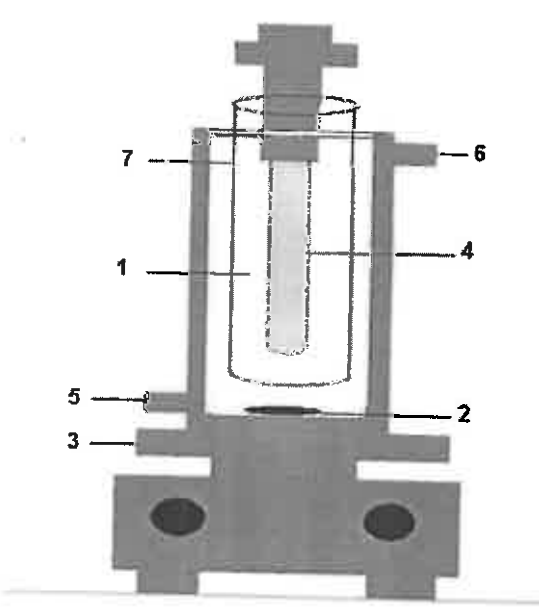


**Fig. 1.** Scheme of the used photoreactor; (1) dye solution; (2) magnetic stir bar; (3) magnetic stirrer, (4) visible lamp; (5) cooling water in; (6) cooling water out; (7) quartz tube.

the precursor was calcined at  $550\,^{\circ}\text{C}$  for 1 h. The bare  $\text{TiO}_2$  was also prepared using a similar method unless urea addition.

The main product, HP/N-TiO<sub>2</sub> nanocomposite, was prepared in the way that the synthesized N-TiO2 (1.0g) was added into  $3.0 \times 10^{-3}\,\text{M}$  of HP solution in ethanol and the suspension was sonicated for 30 min. The mixture was stirred for 48 h at room temperature to obtain the absorption/desorption equilibrium. Finally, the solid was separated by centrifugation, washed several times with ethanol in order to remove the unloaded HP molecules and dried at room temperature. For the aim of activity comparison, HP/TiO2 nanocomposite was also prepared by following the same procedure. The amount of adsorbed HP was estimated by measuring the concentration of the dyes desorbed from the N-TiO<sub>2</sub> surface which was attained by immersing 25 mg of the HP/N-TiO2 samples into 5 mL of NaOH solution (0.1 M) [29,30]. The absorbance of the resulting solution was measured at HP maximum wavelength of 397 nm using a UV-vis spectrophotometer (Jasco-V630) and compared with reference solutions (HP concentrations of: 0.003, 0.006, 0.009 and 0.012 mM in 0.1 M NaOH solutions).

## 2.3. Products characterization and photocatalytic activity

The prepared xerogels were thermally analyzed in air by a PerkinElmer Pyris Diamond apparatus at a scanning rate of  $5\,^{\circ}$ C/min. All samples were analyzed by a Structures-APD 2000 X-Ray Diffractometer using Cu K $\alpha$  radiation ( $\lambda$ =0.15406 nm) radiation in the  $2\theta$  range of 10-80 $^{\circ}$ . The crystalline size of  $TiO_2$  was determined according to the Scherrer equation using the full-width at half maximum (FWHM) of peak broadening. The FT-IR spectra were recorded on a PerkinElmer 65 spectrophotometer. Specific surface area of the sample was measured by BET method on Phschina 1020 at  $-196.15\,^{\circ}$ C nitrogen adsorption-desorption mode. The UV-vis spectra of  $TiO_2$  samples in the 200–1100 nm were recorded. The morphology of hybrid nanocomposite was determined using Zeiss-Sigma field emission scanning electron microscopy.

Photodegradation of MO in the presence of photocatalyst products was examined in a Pyrex reactor with a magnetic stirring bar and water circulating jacket (Fig. 1). The visible light source

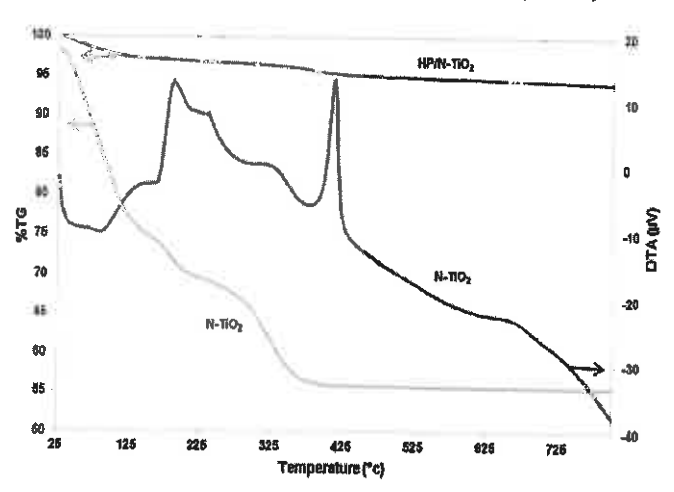


Fig. 2. TGA curves of the N-TiO $_2$  dry gel and HP/N-TiO $_2$  nanocomposite, and DTA curve of the N-TiO $_2$  dry gel.

was an Osram HCI-T 150 W metal halide lamp [31] (light intensity specification presented in Fig. S1), placed centrally in the reactor. The HP/N-TiO<sub>2</sub> nanocomposite (0.3 g) was added to 300 mL of MO solution (5.0 mg/L). In order to reach the adsorption–desorption equilibrium, the suspension was magnetically stirred in dark for 1 h, and the lamp was then switched on. The suspension was sampled at regular time intervals and rigorously centrifuged for 10 min to separate suspended nanoparticles and the concentration of MO was immediately analyzed. For comparison, the MO degradation experiment was conducted under the same conditions with each of N-TiO<sub>2</sub>, HP/TiO<sub>2</sub> and bare TiO<sub>2</sub> nanoparticles as photocatalysts. The role of HO\* radicals on the degradation of MO was determined by adding mannitol (0.1 M) as HO\* scavenger.

#### 2.4. Analytical method

The absorption spectrum of methyl orange shows a peak at 464 nm. The change of absorbance at this maximum wavelength indicates the MO degradation. The UV absorbance of the samples was measured by means of a UV-vis spectrophotometer (UV, Jasco-V630) and using the appropriate calibration curve (Fig. S2). The degradation efficiency was then calculated from  $[(C_0 - C_t)/C_0] \times 100$ , where  $C_0$  and  $C_t$  denote the appropriate MO concentration at initial and any reaction time, respectively.

#### 3. Results and discussion

#### 3.1. Surface and structure characteristics of the samples

TG-DTA curve of the dried gel of N-doped TiO2 nanoparticles and TGA diagram of HP/N-TiO2 nanocomposite are shown in Fig. 2. The TG curve of N-TiO2 dry gel includes mainly two steps. The initial weight loss (~25%) appears at the temperature range from room temperature to 150°C. This is attributed to the evaporation of physically adsorbed water and alcohol in the xerogel. The second weight loss (~20%) between 150 and 350 °C corresponds to the combustion of organic compounds like acetyl acetone. In addition, the DTA curve reveals exothermic peaks at 425 and 700 °C. These can be attributed to the anatase phase formation and anatase to rutile phase transformation, respectively. Several endothermic and exothermic peaks are observed before 425 °C, which means that the calcining process of the composite gel includes a series of dehydration, decomposition and combustion/oxidation reactions [32]. For the HP/N-TiO2 nanocomposite the TGA diagram shows that the loss of weight follows two steps. The first step (~3.5%) occurs from 25

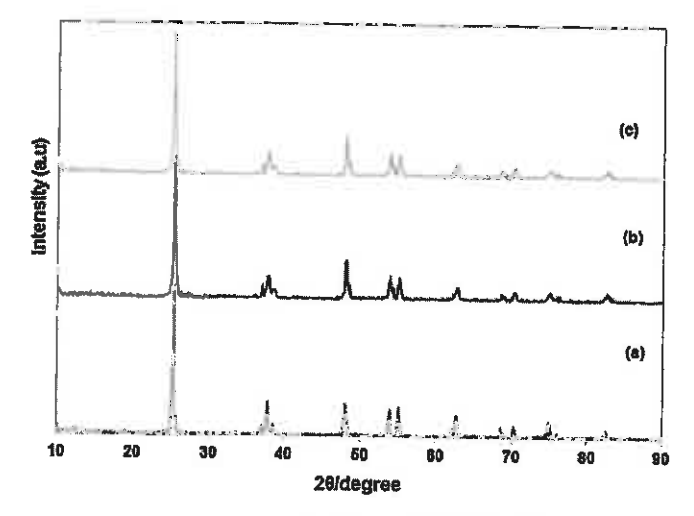


Fig. 3. XRD patterns of bare  $TiO_2$  (a), N- $TiO_2$  nanoparticles (b) and HP/N- $TiO_2$  nanocomposite (c).

**Table 1** Crystallite sizes and  $E_g$  values of the synthesized products.

Product	Size (nm)	Eg (eV)	
bare TiO <sub>2</sub>	40.4	3.26	
N-TiO <sub>2</sub>	29.7	2.91	
HP/N-TiO <sub>2</sub>	29.8	2.53	

to  $125\,^{\circ}\text{C}$  which could be attributed to the evaporation of physically absorbed water and alcohol molecules. During the second loss ( $\sim$ 2.5%), within the range of  $125-450\,^{\circ}\text{C}$ , organic matters such as HP are combusted.

XRD analysis was carried out to investigate the crystal identity of  ${\rm TiO_2}$  samples and the effect of nitrogen and HP on the crystal structure of  ${\rm TiO_2}$ . The XRD patterns of bare  ${\rm TiO_2}$ , N-TiO<sub>2</sub> nanoparticles and HP/N-TiO<sub>2</sub> nanocomposite samples are shown in Fig. 3. XRD patterns of all samples demonstrate the anatase phase as the sole crystalline phase. It can be seen that the diffraction peaks of anatase phase widen and their intensity is weakened with N doping, showing the lower crystallinity and smaller size nanoparticles. No new diffraction peaks are observed in the N containing phase. The close ionic radius of N³- (0.171 nm) and O²- (0.144 nm) leads to the substitution of oxygen by nitrogen [33]. Using Debye–Scherrer's formula, the size of the particles was calculated from the [101] diffraction peak as [34]:

$$d = \frac{0.9\lambda}{\beta \cos \theta} \tag{1}$$

where d is the particle size,  $\lambda$  is the X-ray wavelength corresponding to Cu K $\alpha$  radiation (0.15406 nm),  $\beta$  is the full width at half maximum (FWHM) of the XRD peak and  $\theta$  is the diffraction angle. The crystallite sizes are listed in Table 1. The obtained size of N-TiO<sub>2</sub> sample is smaller than that of bare TiO<sub>2</sub>. Peaks of the HP/N-TiO<sub>2</sub> nanocomposite are similar to N-TiO<sub>2</sub> nanoparticles. The diffraction peaks of HP were not detected in the hybrid nanocomposite which could be assigned to its complete dispersion into TiO<sub>2</sub> nanoparticles and low loading quantity. The peak position and peak width of HP/N-TiO<sub>2</sub> is same as that of N-TiO<sub>2</sub>, indicating that the HP adsorbed on the surface of N-TiO<sub>2</sub> has no influence on the crystal structure and particle size of the N-TiO<sub>2</sub> catalyst [13,17,35].

The FT-IR spectra of pure HP, TiO<sub>2</sub>, N-TiO<sub>2</sub> and HP/N-TiO<sub>2</sub> samples are shown in Fig. 4. The broad band at low wavenumber range from 400 to 800 cm<sup>-1</sup> can be ascribed to the strong stretching vibrations of Ti—O bond. Meanwhile, the intensity of IR band related to Ti—O—Ti vibration mode in pure TiO<sub>2</sub> sample is increased com-

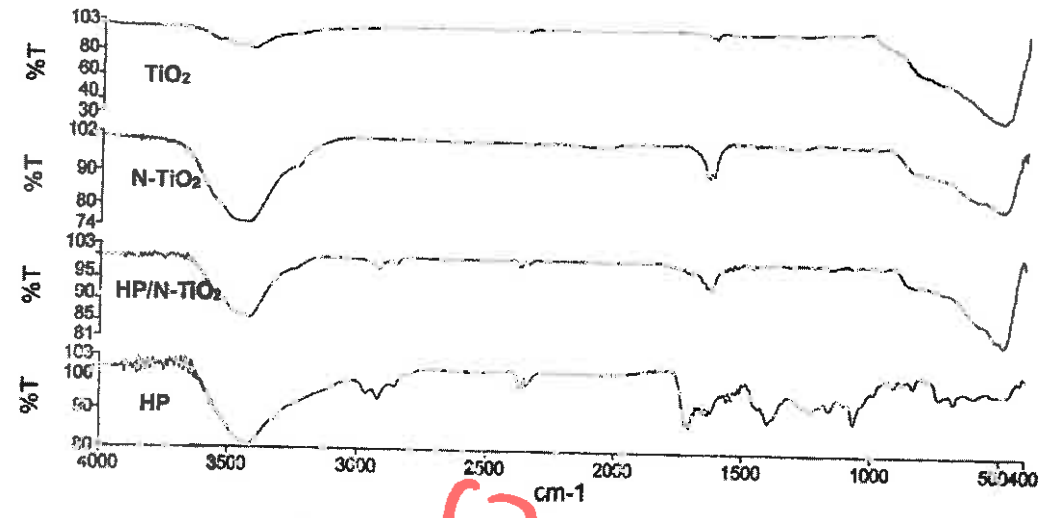


Fig. 4. FT-IR spectra of TiO2, N-TiO2 and HP/N-TiO2 nanoparticles and HP.

pared with N-TiO<sub>2</sub>, indicating that the corresponding anatase TiO<sub>2</sub> crystallinity is decreased [36] as nitrogen is doped on TiO<sub>2</sub>, in accordance with the XRD analysis. Additionally, two main peaks located at 3415 and 1620 cm<sup>-1</sup> can be assigned to the stretching and bending vibration of hydroxyl group on the catalyst surface and water absorbed on the surface [37]. It is well known that hydroxyl groups play an important role in photocatalytic reaction. Comparing the obtained spectra, it is revealed that the intensity of the two absorption bands in the N-TiO<sub>2</sub> sample assigned to the hydroxyl groups is stronger than that in bare TiO<sub>2</sub>, indicating that doping with nitrogen favors the increase of hydroxyl groups, which was considered beneficial for the photocatalytic process [36].

After immobilization of HP on N-TiO2, the basic characteristic peaks for TiO2 is hardly changed. The stretching vibrations of C-C, C—H bonds can also be observed in the supported catalyst, indicating the presence of HP on the surface of N-TiO2. Further, the spectra show that the peaks corresponding to the stretching vibrations of hydroxyl groups are broader and stronger in N-TiO2 than that of supported catalysts, due to the decrease of hydroxyl groups after HP immobilization [38]. The dye used in this study, HP, contains two carboxylic groups, which possesses strong binding ability to the surface of N-TiO<sub>2</sub> through the O=C-O-Ti bonds. For the pure dye, stretching frequencies of the carboxylic group are located at 1710 and 1440 cm<sup>-1</sup> for the antisymmetric and symmetric stretching vibrations, respectively. After coordinating to N-TiO $_2$  surface, the stretching frequencies of the carboxylic groups are located at 1660 and 1452 cm<sup>-1</sup> for the antisymmetric and symmetric stretching vibrations, respectively, providing clear evidence for deprotonation of the carboxylic group upon addition of N-TiO $_2$  nanoparticles. The frequency difference between the antisymmetric and symmetric stretching vibration ( $\Delta = v_{asym} - v_{sym}$ ) is useful in identifying the binding mode of the carboxylate ligand [39]. Therefore, the  $\Delta$ value estimated for HP loaded on the N-TiO  $_2$  is found to be  $208\,cm^{-1}$  $(1660 - 1452 = 208 \text{ cm}^{-1})$ , which is a smaller value than that of the pure HP (270 cm<sup>-1</sup>) and suggests that the binding mode of HP on N-TiO2 is predominantly bidentate (Fig. 5).

The surface area of the N-TiO<sub>2</sub> and TiO<sub>2</sub> nanoparticles, based on BET measurements, were 24.46 and  $18.32\,\mathrm{m}^2/\mathrm{g}$ , respectively. The incorporation of nitrogen ionic increases the extent of the surface area [35,40]. These results are consistent with the results of XRD analyses. The amount of HP adsorbed onto N-TiO<sub>2</sub> and TiO<sub>2</sub> powders was found to be 21.29 and 13.49  $\mu$ mol/g, respectively (see Section 3.2). The adsorption amount of HP on N-TiO<sub>2</sub> is higher than

Fig. 5. Schematic illustration of bidentate binding of HP on N-TiO<sub>2</sub>.

that of TiO<sub>2</sub>. When particle diameter decreases, the quantity of TiO<sub>2</sub> increases per unit mass, i.e. dye loaded sites should increase [41].

The effect of N-doping and HP loading on the band structure and band gap energy is shown by absorbance spectra (Fig. 6). The visible absorption spectra illustrate that the N-doped TiO<sub>2</sub> is a photocatalyst with the capability of photocatalysis under visible light irradiation. Furthermore, the prepared N-TiO<sub>2</sub> sample has absorption band at visible light region and that the band gap energy of N-doped TiO<sub>2</sub> was lower than that of anatase TiO<sub>2</sub>. The band gap energy of the samples were determined by the following equation [42]:

$$E_{g} = \frac{1239.8}{\lambda} \tag{2}$$

where  $E_{\rm g}$  is the band gap (eV) and  $\lambda$  (nm) is the wavelength of the absorption edge in the spectrum. Compared with bare TiO<sub>2</sub>, the band gap was changed from 3.26 to 2.91 eV. In a previous study it was showed that the reduction of the width of band gap of TiO<sub>2</sub> is attributed to the inclusion of nitrogen and the presence of oxy-

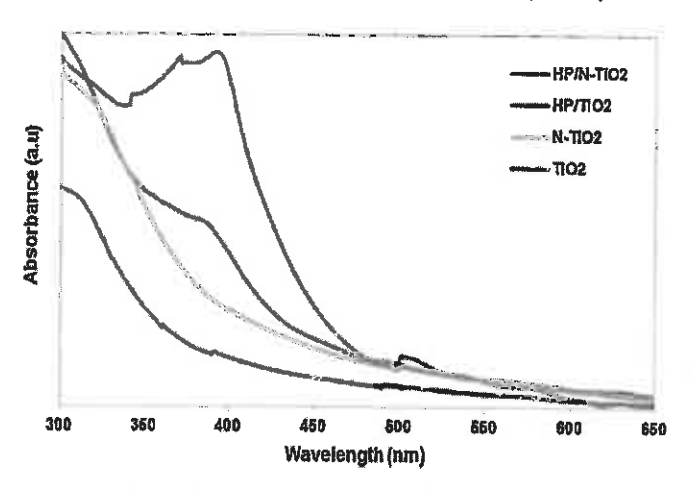


Fig. 6. UV-vis absorption spectra of different samples.

gen defects in the structure [12]. It could be educed that mix of the O 2p states and substituted N 2p contributes in the band gap narrowing. This narrower bandgap will facilitate the transfer of electron from valance band to conduction band in the doped oxide semiconductor under visible light illumination, which can result in higher photocatalytic activities [13,43]. Thus it can be expected that the N-TiO<sub>2</sub> photocatalyst would demonstrate better photocatalytic activity than pure TiO<sub>2</sub>. Obviously, there is no absorption above 400 nm for TiO<sub>2</sub>, while the HP/TiO<sub>2</sub> and HP/N-TiO<sub>2</sub> nanocomposites exhibit the characteristic peaks of HP, indicating that HP successfully is loaded onto the TiO<sub>2</sub> surface while the porphyrin framework has been safely maintained. These characteristic bands were attributed to HP's Soret band and Q-band absorption [41]. Val-

ues of the band gap energies of products ( $E_g$ ) have been reported in Table 1, where a red shift in the visible region from 3.26 to 2.53 eV for the bare  $TiO_2$  and  $HP/N-TiO_2$  photocatalyts respectively, can be seen. HP makes  $TiO_2$  and  $N-TiO_2$  to have a strong absorption in the region of 350–500 nm. The absorption intensity of  $HP/N-TiO_2$  nanocomposite is much higher than that of  $HP/TiO_2$  in the region of 350–500 nm which confirms the higher dye loading.

In order to determine the complex formation between the anchoring group of HP and N-TiO<sub>2</sub>, we have conducted studies using UV-vis spectroscopy that is shown in Fig. S3. The HP in ethanol solution exhibits a strong Soret absorption at 397 nm together with weak Q bands between 500 and 700 nm [44]. It was therefore found that the absorption bands of the HP coupled N-TiO<sub>2</sub> are all red shifted relative to those of the HP in ethanol solution. The red shift of the Soret band is reasonable to conclude that HP/N-TiO<sub>2</sub> nanocomposite is formed by the covalent binding of N-TiO<sub>2</sub> and anchoring groups of HP rather than only physical adsorption [45]. Thus the change in the absorption spectra again confirms the formation of the HP/N-TiO<sub>2</sub> complex. The UV-vis absorption spectrum of the HP/N-TiO<sub>2</sub> nanocomposite was also obtained after 1 month in the dark. The UV spectrum of the aged sample was kept unchanged compared to the fresh sample, indicating that HP/N-TiO<sub>2</sub> was stable.

Scanning electron micrographs were used to show the morphological situation of the N-TiO<sub>2</sub> and HP/N-TiO<sub>2</sub> powders. As shown in Fig. 7(a), the N-TiO<sub>2</sub> has a lumpy structure, and its surface is smooth. After being treated with HP solutions, shown by Fig. 7(c), N-TiO<sub>2</sub> loads porphyrin and the surface contains irregular particles and becomes rough. The micrograph of N-TiO<sub>2</sub> with a roughly 37.9 nm diameter can also be seen in Fig. 7(b) indicating almost spherical shapes. When HP is loaded on the surface of N-TiO<sub>2</sub>, aggregates could be observed clearly from the micrographs of HP/N-TiO<sub>2</sub>, as

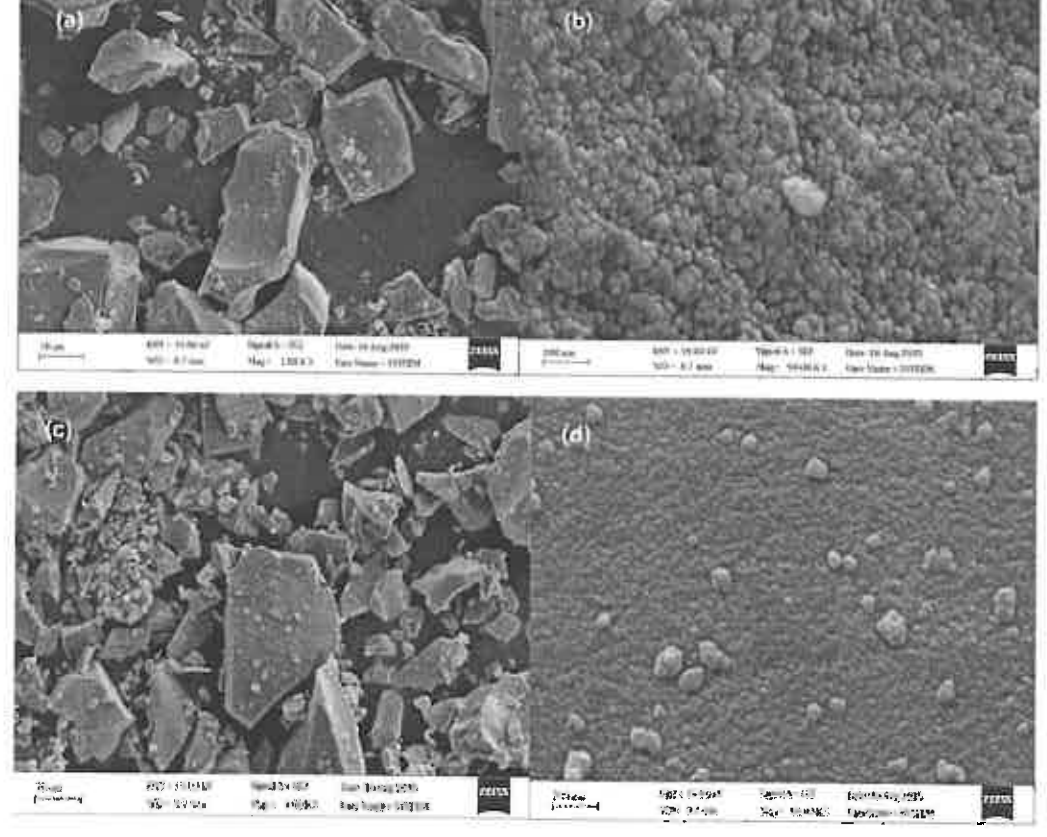


Fig. 7. SEM micrographs of N-TiO<sub>2</sub> (a,b) and HP/N-TiO<sub>2</sub> (c,d) products with different magnifications.

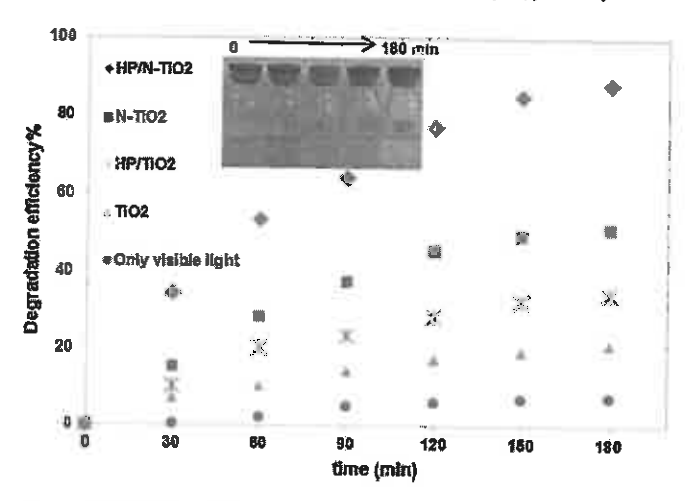


Fig. 8. Degradation efficiency vs. irradiation time of MO with different photocatalysts under visible light irradiation,  $[TiO_2] = [N-TiO_2] = [HP/TiO_2] = [HP/N-TiO_2] = 1.0 g/L$ ; MO initial concentration = 5 mg/L. (inset is the image of the changes in the color of MO under visible-light illumination).

shown in Fig. 7(d). This indicates the strong adsorption occurred between HP and the TiO<sub>2</sub> support. As well, after HP impregnation, the micrograph of the HP/N-TiO<sub>2</sub> is blurred and the visualization of the N-TiO<sub>2</sub> structure is not clear. This confirms the presence of HP on the surface of N-TiO<sub>2</sub>.

#### 3.2. Photocatalytic activity of products

The photocatalytic activity of the samples was evaluated by measuring the degradation of the organic dye MO under visible light irradiation, Fig. 8 shows the degradation efficiency with reaction time without any catalyst as well as in the presence of bare TiO2, N-TiO2 and HP/N-TiO2 samples. The direct visible light illumination without any catalyst can lead to only about 7.0% degradation within 180 min, whereas bare TiO2 nanoparticles exhibited 21.2% degradation of MO under the same conditions. This can be accounted presumably to the self-sensitization capability of MO molecules [46]. Using N-TiO2, however, can lead the degradation to enhance to about 51.4% degradation, and use of HP/TiO2 gave an efficiency of 33.1%. The improvement of the catalytic activities through N-doping is due to the narrowed band gap of TiO2, as was mentioned in the previous section. After sensitizing N-TiO2 by HP, much higher photoactivity was obtained so that degradation efficiency reached to 88.5%. It can be calculated, therefore, that the photocatalytic activity, after sensitizing of bare TiO2 and N-TiO2 samples, enhances to about 1.7 times. Interestingly, the photocatalytic activity increment of HP/N-TiO2 compared with bare TiO2 is more than the sum of increments coming from dye sensitization of just TiO2 and N-TiO2. This result indicates a synergism effect between HP sensitization and nitrogen doping.

To investigate the role of MO initial concentration, different amounts of this dye were utilized under similar operating conditions. Results (Fig. S4) show a decreasing trend of degradation with initial concentration which is expected due to limited photocatalyst surface area and the light emission in contact with concentrated solutions.

The rate of the heterogeneous photocatalytic degradation of MO (5 mg/L initial concentration) has been described with the Langmuir–Hinshelwood kinetic model which can be expressed as [47]:

$$r = -\frac{dC}{dt} = \frac{kK_{ad}C}{1 + K_{ad}C} \tag{3}$$

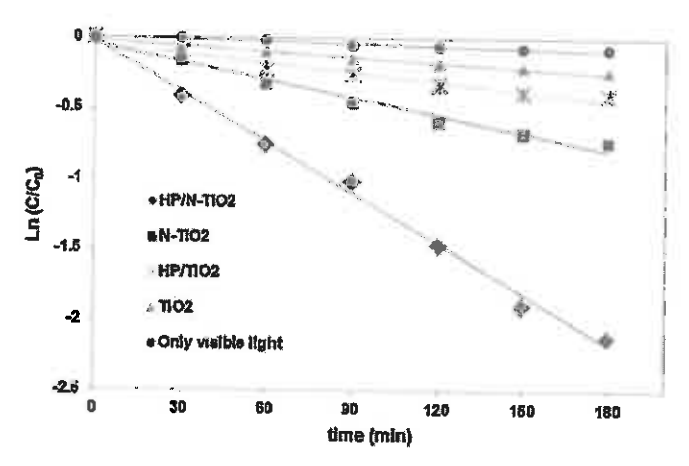


Fig. 9. The kinetics of MO photocatalytic degradation with different photocatalysts under visible light irradiation,  $[TiO_2] = [N-TiO_2] = [HP/TiO_2] = [HP/N-TiO_2] = 1.0 g/L$ ; MO initial concentration = 5 mg/L.

**Table 2**Kinetic parameters for the photocatalytic degradation of MO under visible light.

Case	No catalyst	Bare TiO <sub>2</sub>	N-TiO <sub>2</sub>	HP/TiO <sub>2</sub>	HP/N-TiO₂
k <sub>app</sub> (min <sup>-1</sup> )	0.0005	0.0013	0.0042	0.001	0.012
t <sub>1/2</sub> (min)	1386	533,2	165	693.1	57,8

where r represents the initial rate of photooxidation, C is the MO concentration at any time t,k is the reaction rate constant, and  $K_{\rm ad}$  is the adsorption coefficient of the MO molecules on photocatalyst. At the low concentrations of MO ( $K_{\rm ad}C$ <<1) which is the case in this work, Equation (3) can be simplified to an apparent first order equation:

$$\ln \frac{C}{C_0} = -kK_{\rm ad}C = -k_{\rm app}t$$
(4)

where  $k_{\rm app}$  =  $kK_{\rm ad}$  is the apparent rate constant and  $C_0$  is the initial concentration of MO. In order to evaluate qualitatively the rate of photodegradation of MO under visible light illumination, the linear relationship of the natural logarithm of the ratio between the initial concentration of MO and its concentration at different times (lnC/ $C_0$ ) versus the corresponding irradiation time is presented in Fig. 9. The results indicate that the photocatalytic degradation of MO can be described by the apparent first order kinetic model. Kinetic parameters for the photocatalytic degradation of MO are listed in Table 2.

Previous studies indicate that hydroxyl radical, HO\*, was the major oxidant for photocatalytic degradation in wastewater treatment [20]. To determine the contribution of HO\* radical on degradation, mannitol scavenger (0.1 M) was added to HP/N-TiO2 aqueous dispersion. In comparison with the main reaction (no scavenger), the MO degradation decreased to about 58% (Fig. S5) which is due to hydroxyl radical scavenging by mannitol. These results indicate that the hydroxyl radical has a significant contribution of about 42% while the peroxyl radical ( $O_2^{\bullet-}$ ) and the reactive holes provide the remaining activity.

The photocatalytic mechanism of N-TiO<sub>2</sub> sensitized by HP can be deduced based on above discussions and is shown schematically in Fig. 10. When the visible light irradiates on the surface of HP/N-TiO<sub>2</sub> nanocomposite, the electrons can be produced via two different paths. In one path, nitrogen doping can modify the band structure of TiO<sub>2</sub> by creating the intra-band-gap states close to the valence band edges, and the flat band potential finds a level higher than that of the conduction band of pure TiO<sub>2</sub>. Thus, when the visible light irradiates on the surface of the N-TiO<sub>2</sub>, the electrons can be excited easier from the intra-band-gap states to flat band [13].

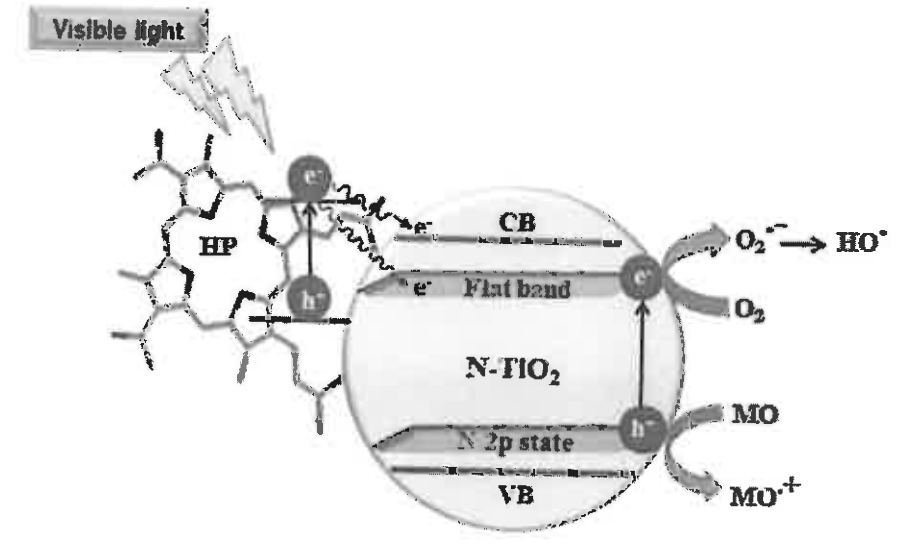


Fig. 10. Schematic illustration of the proposed mechanism for N-TiO $_2$  sensitized by HP in photocatalytic degradation.

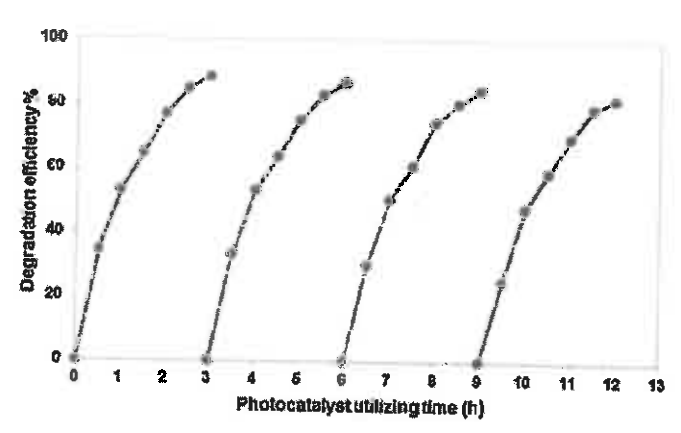


Fig. 11. Four consequtive cycles of photocatalytic degradation of MO; [HP/N-TiO<sub>2</sub>] =  $1.0\,\text{g/L}$ ; MO initial concentration =  $5\,\text{mg/L}$ .

On the other path, the HP on the surface of the N-TiO $_2$  nanoparticles generates photo-induced electrons by absorption of visible light. Then the photo-induced electrons transfer to the conduction band or flat band of N-TiO $_2$ . Meanwhile HP cationic form (HP $^+$ ) gets the electrons from the solution to reproduce HP. The reactive electrons present on the conduction band and flat band of N-TiO $_2$  can reduce adsorbed O $_2$  molecules on the surface of TiO $_2$  to peroxyl radical (O $_2$  " $^-$ ), which in-turn become highly oxidative hydroxyl radical (HO $^+$ ) through a series of reactions, resulting in the oxidation of MO, as the final step [48]. Meanwhile, the reactive holes can oxidize MO to its radical cation either directly or through a primarily formed HO $^+$  produced by the oxidation of water. The synergistic effect of the HP sensitization and nitrogen doping make HP/N-TiO $_2$  catalyst to exhibit accelerated photoexited electron transfer and therefore so much degradation.

#### 3.3. Catalyst stability evaluation

In order to investigate the stability, the repeating use of the HP/N-TiO<sub>2</sub> nanocomposite for MO degradation was investigated. At the end of each experiment, the solution residue from the photocatalytic degradation was filtered and the HP/N-TiO<sub>2</sub> sample was washed and dried. The dried catalyst sample was used again for the degradation of MO under identical experimental conditions. The results show a very mild decrease (Fig. 11), confirmed that HP/N-

 ${
m TiO_2}$  catalyst can be recycled at least four times without significant loss of activity. At the first time of HP/N-TiO<sub>2</sub> usage, 88.5% degradation of MO was achieved and after four cycles, the degradation efficiency retained as high as 82.1%. In addition, in UV-vis spectra (Fig. S6), it is clear that the characteristic peak of HP remains the same after four times repeating usage of the photocatalyst and that the bind between N-TiO<sub>2</sub> and HP is still strong and is not separated by dissolution. So, the HP/N-TiO<sub>2</sub> is an efficient and stable photocatalyst, merit for the degradation of organic pollutants in water under visible irradiation.

#### 4. Conclusions

In summary, titania and nitrogen-doped titania (N-TiO2) nanoparticles were sensitized by HP for improving the visiblelight response. The new hybrid nanocomposite was methodically characterized with the aid of standard optical and microscopic techniques. Accordingly, UV-vis absorbance analysis of the prepared nanocomposite indicated that HP in hybrid nanocomposite extends the absorption of N-TiO2 into the visible region such that visible light could be harnessed. FT-IR analysis also indicated successful binding of the dye to the N-TiO2 surface. Due to the presence of carboxyl groups, HP can be chemisorbed on the surface of N-TiO<sub>2</sub> nanoparticles through the O=C-O-Ti bonds. Examining the photocatalytic activity of the hybrid nanocomposite on degradation of methyl orange under visible light showed superior degradation over pure N-TiO2 and TiO2 (about 4.2 and 1.7 times enhancement, respectively, compared with bare TiO2). This high visible light activity of HP/N-TiO2 can be attributed to the synergistic effect of titania nitrogen doping and sensitization with HP.

#### Acknowledgement

The authors wish to acknowledge the Bu-Ali Sina University authorities for providing the financial support to carry out this work.

#### Appendix A. Supplementary data

Supplementary data associated with this article can be found, in the online version, at http://dx.doi.org/10.1016/j.molcata.2015.12.

#### References

- [1] Y. Lv. L. Yu. H. Huang, H. Liu, Y. Feng, Preparation, characterization of P-doped TiO<sub>2</sub> nanoparticles and their excellent photocatalystic properties under the color light irradiation, J. Alloy. Compd. 488 (2009) 314–319.
- [2] X. Qiu. C. Burda, Chemically synthesized nitrogen-doped metal oxide
- [3] H. Diver, C. Variikli, K. Mizzait, A. Dana, Characterizations and photocatalytic activity comparisons of N-doped nc-TiO<sub>2</sub> depending on synthetic conditions and structural differences of amine sources, Energy 56 (2011) 1242–1254.
   [4] S. Balazubramandau, P. Wang, R.D. Schaller, T. Bajli, E.A. Bonhkova.
- High-performance bloassisted nanophotocatalyst for hydrogen production. Nano Lett., 13 (2013) 3305-3371.
- [5] Y. Fare, Z. Li, B. Yane, S. Xu, X. Hu, Q. Liu, D. Han, D. Lu, Effect of dve structure on optical properties and photocatalytic behaviors of squaraine-sensitized
- iiC<sub>2</sub> nanocomposite., J. Phys. Chem. C 118 (2014) 16113-16125. [6] H. Hugag, D. Li, Q. Lin, Y. Shao, W. Chen, Y. Hu, Y. Chen, X. Fu, Efficient photocala lytic activity of PZT/TiO2 heterojunction under visible light irradiation, J. Phys. Chem. C 113 (2009) 14264-14269.
- [7] Z. Zhang, C. Shao, X. Li, Y. Sen, M. Zheng, J. Mu, P. Zhang, Z. Guo, Y. Liu, Hierarchical assembly of ultrathin hexagonal SnS<sub>2</sub> nanotheets onto electros pun TiO2 nanofibers: enhanced photocatalytic activity beard on pliptoinduct.d interfacial charge transfer, Nanoscale 5 (2013) 666-618.
- M. In hoper, V. Atonf, Study of the photocatalytic activity of nanonystalline 5, N-codoped TiO<sub>2</sub> thin filter and powders under visible and numlight irradiation, Appl. Surf. Sci. 258 (2012) 6595–6601.
- [9] Z. Mesyari, M. Gharagorlov, A. Khosravi, K. Gharanjig, Synthesis characterization and evaluation of efficiency of new hybrid Pc/Fe-TiO2 named unposite as photocatalyst for decolorization of methyl orange using visible light irrediation, Appl. Cata. A: Gen. 411–412 (2012) 136–145.
- [10] A.L. Lipsebigler, G. Lu, J. T. Yates Jr., Photocatalysis on TiO<sub>2</sub> surfaces: principles, mechanisms, and relected results. Chem. Rev. 95 (1995) 735–738.
- [11] R. Assiai, T. Morikawa, T. Ohwaki, K. Aoki, Y. Taga, Visible-light photocatalysis in nitragen-doped (itanium oxide). Science 293 (2001) 265–271.
- [12] G. Caurados Olivero , E.A. Fárz- Vozo, F.M. Ortiva, C. Ferrou eto, L-M. Chevelor, Degradation of atrazina using metalloporphyvini supported on Tio, under visible light irradiation. Appl. Catal. 8: Environ. 40 (2009) 448-45-4.
  [13] K. Del Ángal-Sanchez, O. Vizquez-Cuchillo, A. Armilar-Eigenschal, A.
- Chiz-López, A. Herreta-Gémez, Photocatalytic dugradation of 2.4-dichlorophenoxyacetic acid under visible light; affect of synthesis route, Mater, Chem. Phys. 139 (2013) 423-430.
- [14] W. Jiri Likipontorn, S. Thachepan, A. Songsasen, Photodegradation of ph mantitrene by N-doped TiO2 photocatalyet, J. Environ. Sci. Health Part A 44 (2009) 041-046
- [15] G. Yang, Z. Jiang, H. Shi, T. Aiao, Z. Yan, Preparation of highly visible-light active (1-dop.d TiO2 photocatalyst, J. Mater. Chem. 7.9 (2010) 5301.
- [16] C. Di Valentin, E. Linazzi, G. Purchioni, A. Selloni, S. Livraghi, M.C. Paganini, E. Girmello, N-doped TiO: theory and experiment, Chem. Phys. 335 (2007)
- [17] X. Yang, C. Cao, L. Enckson, K. Honn, R. Maghirang, X. Hlabunde, Proto-catalytic degradation of rhodamine B on C-, S-, N-, and Fe-doped TiO<sub>2</sub> unal r visible-light irradiation, appl. Catal. B: Environ. 91 (2009) 657-002.
- [18] M. Kitano, M. Matsuoka, M. Deshima, M. Anpo, Recent developments in titradich, oxide-based photocatalysts, Appl. Catal. A: Gen. 525 (2007) 1–14.
   [19] M.K. Mazcer addin, C. Klein, P. Liske, M. Grätzel, Synthesis of novel ruthenium
- sensitizers and their application in dyc-sensitized solar cells, Coord. Chem. Nav. 245 (2001) 1460–1467.
- [20] J.-H. Yum, P. Walter, S. Huber, D. Rentsch, T. Geiger, F. Müesch, F. De Angelia, M. Grazel, M.L. Hazaraddin, Efficient for red sansi ization of nanocapitalling TiO falms by an unsymmetrical squarative dye, J. Am. Chem. Soc. 125 (2007) 10320-10321.
- [21] D. Liten, D. Yang, J. Gente J. Zhu, Z. Jiang, Improving visible-light
- D. Chen, D. Yato, J. Geros, J. Zitt, Z. Beng, unproving, v. Bue-ngm photo: "Jytic activity of H-doped TiC<sub>2</sub> nanopurticles via sensitization by Zn porphyrin, rapk. Sum. Sci. ToD (2008) 2879–2884. K. Wonnedharee, V. Missyon, S. Chavashij, Dye-sensitized rolar cell using natural three cardiocted from rosella and blue pea three re, Sol. Energy Mater. Sol. Cell: 91 (2007) 556-571.
- [23] C.W. Latker, F.R. Sch-ffer, M.B. Fereira, E.R. Teixeira, D. J. Weibel, Faoto: militing degradation of organic dyes by visible light using riboflavir. adsorbed a 1th autility of TiO: Nonotubes, J. Braz. Chem. Soc. 25 (2014) 2417-2434
- [24] G.J. Moyer, Molecular approaches to solar energy conversion with coordination consolunds anchored to sendoor ductor surfaces, Inorg. Claum, 44 (0.005) 6862-6864,

- [25] J. Shang, F. Zhao, T. Zhu, J. Li, Photocatalytic degradation of rhodamine B by dye-centitized TiO2 under visible-light irradiation, Sci. Chin. Chem. 54 (2011) 167-172
- [26] P. Kar, S. Sardar, E. Alarousu, J. Sun, Z.S. Seddigi, S.A. Ahmed, E.Y. Danish, O.F. Mohammed, S.K. Pal, Impact of metal ions in porphyrin-based applied materials for visible-light photocatelysis: key information from ultrafast. electronic upectroscopy, Chemistry 20 (2014) 10475-10483.
- 5.iv. Reda, Stubility and photodegradation of phthalocyanines and hematoporphyrin doped PMMA as solar concentrators, Solar Energy 81 (2007) 755-760.
- P.F. Schwacz, N.J. Turro, S.H. Dosomann, A.M. Braun, A.-M.A.A. Wahab, H. Duarr, A new method to determine the generation of hydroxyl radicals in illuminated TiO<sub>2</sub> suspensions, J. Phys. Chem. B 101 (1997) 7127–7134.
- S. Kohtani, S. Niehioka, E. Yoshioka, H. Miyabe, Dye-sensitized photo-hydrogenation of aromatic ketones on titanium dioxide under visible light irradiation, Catal. Commun. 43 (2014) 61-65.
- [30] H.-S. Yoon, X.-H. Ho, J. Jang, H.-J. Lee, S.-J. Kim, H.-Y. Jang, N719 dye-sensitized organophotocatalysis: enantioselective random michael addition/oxyamination of aldehydins, Org. Lett. 14 (2012) 3272-3775.
- [31] Osrani.com (September) (2015), retrieved from http://www.osram.com/ orann\_com/products/lamps/high-intensity-discharge-lamps/metal-halidelamps-with-ceramic-technology/powerball-hci-t/index.jsp.
- [32] K. Elehniji, M. Kalbi, E. Elaloui, Sol-get reverse micelle preparation and characterization of N-doped TiO<sub>2</sub>: efficient photocatalytic degradation of methylene blue in water under visible light, J. Ind. Eng. Chem. 18 (2012) 178-132.
- [33] Y. Su, Y. Xiao, Y. Li, Y. Du, Y. Zhang, Preparation, photocatalytic performance and electronic structures of visible-light-driven Fe-E-codoped TiO<sub>2</sub> nanoparticles, Mater. Chem. Phys. 126 (2011) 761–768.
- [34] H.S. Lipson, H. Steepic, Interpretation of X-ray Powder Diffraction Patterns, Macmillan, St Martin & Press, 1970.
  [35] Y. Li, C. Xie, S. Peng, G. Lu, S. Li, Eosin Y-sensitized nitrogen-doped TiO<sub>2</sub> for
- efficient visible light photocatalytic hydrogen evolution, J. Mol. Catal. A:
- Chem. 282 (2003) 117–123.

  X. Chem. 282 (2003) 17–123.

  X. Chem. 3. Yu. Z. Xing, Characterization and mechanism analysis of N doped TiO with vicible light response and its enhanced visible activity, Appl. Surf. 10. 258 (2012) 3244–3246.
- M. Chang, X. Yu, Z. Xing. Enhanced photoelectric property and virible activity of nitrogen doped Tios synthesized from different nitrogen dopants, Appl. Surf. Sci. 203 (2013) 204–208.

  M.T. Zhou, H.B. Ji, X.J. Huang, Photocatalytic degradation of methyl orange
- over metalloporphyrins supported on TiO2 degussa P25, Molecules 17 (2012) 1149-1158
- G. Descon, R. Phillips, Relationships between the carbon—exygen stretching frequencies of carboxylato complexes and the type of carboxylate coordination, Coord. Chem. Rev. 35 (1980) 237–250.
  J. Eliu, B. Yho, Y. Chen, C. Peng, R. Yu, J. Zhang, G. Bai, Enlanced photocatalytic
- activity of nitrogen depied TiO<sub>2</sub> photocatalysts sensitized by metallo Co, Ni-porphyrins, Appl. Surf. Sci. 271 (2013) 39–44.
- G. Kato, C. Nichiyama, T. Yabuta, M. Miyauchi, T. Hashimoto, T. Isobe, A. Makajima, S. Matsusnica. Pore size dependence of self-assembled type photonic crystal on dys-sensitized solar cells efficiency utilising chlorine e6, J. Porous Mater. 21 (2013) 165–176.
- [42] B. O'regan, M. Gratzel, A low-cost, high-efficiency solar cell based on dye-sensitized colloidal TiO- films, Nature 353 (1991) 737-740.
- [43] J. Amunpattarachai, P. Kajitvichyanukul, S. Seraphin, Visible light absorption ability and photocaralytic exidation activity of various interstitial N-doped TiO2 prepared from different nitrogen dopants, J. Hazard, Mater, 168 (2069) 255-261.
- [44] R. S. Frastova, V. Anand, W. Carper, A fluorescence study of hematoperphyrin, Appl. Spectrosc. 27 (1973) 444–449.
- [45] S. Sardar, N. Sarkov, M.T. Myint, S. Al-Harthi, J. Dutta, S.K. Pal, Role of central metal icra in heractopolphyrin-functionalized titania in tolar energy
- conversion dynamics. Phys. Chem. Chem. Phys. 15 (2013) 13562–18570.

  [46] L.V. Kon cantinou, T.A. Albanis, TiO<sub>2</sub> assisted photocatalytic degradation of azo dyes in aqueous colution: kinetic and mechanistic investigations; a review, Appl. Catal. B: Er.vi. on. 49 (2004) 1-14.
- [47] A. Houas, H. Lachheb, M. Ksibi, E. Elaloui, C. Guillard, J.M. Herrmann. Photocatalytic degradation pathway of methylene blue in water, Appl. Catal. 6: Environ. 31 (2001) 145-157.
- [48] W. Shelian, F. Yarafun, Y. Yong, L. Junzi, D.A. Ping, Zh.X. Rong, H.Y. Ping, Catalysis of or a nic pollutant photodegradation by metal phthalocyanines immobilized on TiO2 (SiO2, Chin. Sci. Bull. 56 (2011) 965-976.